# Grapefruit juice containing rich hydroxyl and oxygenated groups capable of transforming 1D structure of NiCo2 O4 into 0D with excessive surface vacancies for promising energy conversion and storage applications

Shusheel Kumar, Aneela Tahira, Mélanie Emo, Brigitte Vigolo, Antonia Infantes-Molin, Amerah Alotaibi, Shoyebmohamad Shaikh, Ayman Nafady, Zafar Hussain Ibupoto

# Grapefruit juice containing rich hydroxyl and oxygenated groups capable of transforming 1D structure of $NiCo_2O_4$ into 0D with excessive surface vacancies for promising energy conversion and storage applications

Shusheel Kumar[a], Aneela Tahira[d], Mélanie Emo[e], Brigitte Vigolo[e], Antonia Infantes-Molin[f], Amerah M. Alotaibi[b], Shoyebmohamad F Shaikh[b], and Ayman Nafady[b*], and Zafar Hussain Ibupoto[*c]

[a]Institute of Physics, University of Sindh Jamshoro, 76080, Sindh Pakistan

[b]Department of Chemistry, College of Science, King Saud University, Riyadh 11451, Saudi Arabia

[c]Institute of Chemistry, University of Sindh Jamshoro, 76080, Sindh Pakistan

[d]Institute of Chemistry, Shah Abdul Latif University Khairpur Mirs, Sindh, Pakistan

[e]Université de Lorraine, CNRS, IJL, F-54000 Nancy, France

[f]Department of Inorgnic Chemistry, Crystallography and Mineralogy. (Unidad Asociada al ICP-CSIC), Faculty of Sciences, University of Malaga, Campus de Teatinos, 29071, Malaga, Spain

*__Corresponding authors__: Zafar Hussain Ibupoto& Ayman Nafady

**Email:** zaffar.ibhupoto@usindh.edu.pk; anafady@ksu.edu.sa

## Abstract

Fabrication of an efficient electrode material is highly demanded for obtaining high energy conversion electrochemical system. In this study, we describe a green and innovative approach of using grape fruit juice as a high carrier of reducing and surface modifying agents for manipulating the surface properties of nickel-cobalt bimetallic oxide $NiCo_2O_4$ nanostructures. Different amounts of grape fruit juice were used to discern its role on the morphological and surface vacancies of $NiCo_2O_4$ nanostructures during oxygen evolution reaction (OER). Importantly, the physical characterization revealed the morphological transformation of $NiCo_2O_4$ nanostructures from 1D nanorods to short range 0D nanoparticles. Furthermore, the surface studies have shown that $NiCo_2O_4$ nanostructures prepared with grapefruit juice have high density of surface vacancies and higher amount of $Ni^{2+}$ and a $Co^{2+}$ metallic ions on the surface of $NiCo_2O_4$ compare to pure $NiCo_2O_4$ nanostructures. The OER of electrodes modified with

$NiCo_2O_4$ nanostructures, particularly (sample-2, 2 mL of grape fruit juice) gave rise to an overpotential value of 260 mV at 10 $mAcm^{-2}$ in 1.0 M KOH aqueous solution along with high durability/stability for 40 h. Additionally, the obtained electrochemical impedance spectroscopy value of 80 Ω and active surface area of 18.1$\mu Fcm^{-2}$ attested for the excellent OER performance of $NiCo_2O_4$ nanostructures (sample-2). Eventually, the proven enhancement in surface vacancies, alternation in the mixed oxidation states of both Ni and Co together with the morphological transformation that have been accomplished via the green, simple, and low-cost strategy of using grape juice make it a suitable option for large scale production of wide range of multifunctional metal oxides and related nanostructured materials for plethora of energy conversion and storage applications.

**Keywords:** $NiCo_2O_4$ nanostructures, grape fruit juice, oxygen evolution reaction, asymmetric supercapacitor, surface vacancies

## 1. Introduction

Currently, world is facing challenge of global warming effect mainly caused by the combustion of fossil fuels. The continuous use of fossil fuels for transport, domestic and industrial applications is decreasing the reservoirs of fossil fuels in the universe. The greenhouse gases play a major role for bringing the global warming effect and consequently causing wide range of threats to every ecosystem of our environment [1, 2]. Therefore, researchers paying intense attention towards the strengthening of renewable energy reservoirs through the production of clean and green fuels in order to maintain and save the ecosystem of our environment [3, 4]. The present technologies used for the production of clean energy are solar, hydro, wind, bio mass and geothermal [5-8]. Beside these methods, water splitting either by photochemical or electrochemical is widely used to produce green fuels of hydrogen and oxygen which can be used either directly or in the development of fuels cells. Theoretical thermodynamic overpotential of 1.23V is required to split water into hydrogen and oxygen gases, indicating the high energy barrier and less likely favorable at any cost. Therefore, the only challenge in the field of water splitting is the need of efficient electrocatalysts to reduce the overpotential of water splitting. Hence, electrochemical water splitting (EWS) is widely used

process because of its eco-friendly and economical energy properties for the production of green fuels like hydrogen and oxygen gases.

In principle, water splitting is accompanied by two half-cell reactions including oxygen evolution reaction (OER) and hydrogen evolution reaction (HER). Among them, OER is the highest energy demanding process, as it involves four electrons transfer and has crucial impact on the efficient production of hydrogen gas [9-14]. To date, the efficient OER electrocatalyst belong to noble metal based materials like Ir/Ru/Pt [1, 2] which are scarcely found in nature and not compatible in terms of economy for large scale applications, therefore the research endeavors have focused towards the development of low cost, earth abundant and efficient electrocatalyst based on nonprecious materials. For this reason, wide range of earth abundant materials are considered recently [3-5] . In particular, transition metal based materials have been widely utilized for the design of OER electrocatalyst owing to their unique d-orbital configuration and significant catalytic activities [6, 7]. For instance, nickel and cobalt oxides are actively implemented in OER due to their availability, tunable morphologies and enhanced catalytic performance at nanostructured phase [8, 9]. The spinel oxide phase of nickel and cobalt $NiCo_2O_4$ has been extensively investigated for catalytic applications [15-23]. Beside energy conversion applications of $NiCo_2O_4$ nanostructures, they are currently of great interest for the development of energy storage technologies. Hence, it is highly desired to design an inexpensive, efficient and earth abundant electrode materials based on $NiCo_2O_4$ using new synthetic strategies that yield unique nanostructure architectures for applications in supercapacitors (SCs) technology. The challenge of lower energy density of SCs strongly limits their scale up practical and commercial applications [24-29]. The energy density is highly dependent on the specific capacitance (Cs), which is more likely connected to the configuration of electrode materials [30-32]. For this reason, the controlled preparation and architecture manipulation of electrode materials with favorable structure are very important to exploit the full performance capabilities of OER and SCs. In this context, $NiCo_2O_4$ based electrode material is highly desirable to investigate both OER and SCs due to its spinel structure that comprises mixed metal valence states favorable for swift charge transfer during the electrochemical processes as well as enabling high electrical conductivity [33-35]. In view of these structure-activity features, the catalytic behavior of $NiCo_2O_4$ towards OER or SCs is mainly governed by the morphology of electrode material, which has taken different shapes like nanoparticles [36, 37], microcuboids [38], hollow spheres [39], octahedrons [40], and nanocages [41]. Numerous approaches have been used to enhance the

performance of nickel and cobalt based oxides towards OER activity [42-44]. The choice of grapefruit in the present study is highly supported by the presence of a wide range of chemical components in its juice like isoflavones, flavanols, furanocoumarins and anthocyanidin [45-54]. The most common chemical components that could act as reducing and surface modifying agents for the nanostructured material are found in the relative portion as citric acid (809.70 mg /100 mL), Naringin (160.79 mg /100 mL), Neohesperidin (9.69 mg /100 mL) and ascorbic acid (16.76 mg /100 mL) ascorbic acid [55, 56]. The presence of essential chemical components with high density of hydroxyl groups are shown in Supplementary Scheme 1. These phytochemicals have the proorties like reducing, capping and stabilizing agents, hence they can be highly useful to control the size and shape during the synthesis of nanostructured material. The scenario of rich edge sites of hydroxyl groups could carry open functional sites for the surface modification and alteration of morphology of $NiCo_2O_4$ nanostructures. Additionally, the presence of these natural compounds can decrease the pH of growth solution, which would possibly change the morphology of $NiCo_2O_4$ nanostructures from 1D to 0D structure and modified the surface with favorable electrochemical activity.

These chemical constituents of grapefruit juice can have ability to tune the morphology, electronic structure, create defects, and enhance the catalytic sites of $NiCo_2O_4$ which together will further accelerate the OER kinetics at low energy barrier and boost up the specific capacitance [57, 58]. To the best of our knowledge, there is no report on the use of grapefruit juice for tuning the catalytic features of $NiCo_2O_4$ nanostructures towards OER and SCs applications.

In this study, we utilized the grapefruit juice with different amounts to tailor the catalytic properties of $NiCo_2O_4$ for OER application. Interestingly, we have noted that the grapefruit juice has changed the morphology of $NiCo_2O_4$ from 1D nanorods to short range 0D nanoparticles, created defects in the structure of material, and enhanced the charge transport during electrochemical performance, consequently a significant improvement in the OER activity was achieved via using $NiCo_2O_4$ material.

## 2. Experimental section

### 2.1. Hydrothermal synthesis of nickel cobalt oxide $NiCo_2O_4$ nanostructures using grape fruit juice

Chemicals used for the synthesis of nickel cobalt oxide $NiCo_2O_4$ nanostructures were nickel chloride hexahydrate, cobalt chloride hexahydrate, potassium hydroxide and urea. They were used without further purification. The desired solutions were prepared in the deionized water. The ruthenium oxide was used as reference material during the performance evaluation of as prepared nanostructured materials. The synthesis process was completed in two steps. Nanomaterial was grown through hydrothermal method. In first step, the solution of 0.1M of cobalt chloride hexahydrate, 0.0151M nickel chloride hexahydrate and 0.1M urea was prepared in 100mL of deionized water. Then, fresh grapefruit juice was collected by electric machine juicer. Afterwards, 1mL and 2mL of grapefruit juice was added separately in the nickel-cobalt precursors and both beakers were labeled as sample-1 and sample-2. The pH of growth solution with the use of grapefruit juice 1mL and 2mL was about 6.7 and 5.9 respectively. A third beaker was also prepared with nickel-cobalt precursor without the use of grapefruit juice and it was labeled pure sample and its pH was about 9.5. The uniformity of growth solution was achieved by mechanical stirring. The beakers were sealed with aluminum sheet very tightly and left into the electric oven at $95^0$C for 5h. After the completion of growth process, the precipitates of nanostructured material were collected on ordinary filter paper and washed several times with the deionized water. The collected amount of material was left for 10h. At the end, the calcination in air was performed at $500^0$C for 5h and black powder of $NiCo_2O_4$ was obtained. A brief synthesis process is represented by Supplementary scheme 2.

The morphology, crystal arrays, chemical composition and surface characterizations of $NiCo_2O_4$ nanostructures were done by different analytical techniques including scanning electron microscope (SEM) at an accelerating voltage of 15kV, X-ray diffraction (XRD) technique with Cu $K_\alpha$ radiation (Cu $\lambda_{K\alpha}$ = 1.5406 Å), high resolution transmission electron microscopy (HRTEM) at 200kV, Tecnai G2 F20, FEI, energy dispersive spectroscopy (EDS), and X-ray photoelectron spectroscopy (XPS) with an Al $K_\alpha$ X-ray resource at 30eV. The binding energy was compared the standard C1s peak at 284.6eV.

### 2.2. Prepared $NiCo_2O_4$ nanostructures towards oxygen evolution reaction

Electrochemical measurements of various $NiCo_2O_4$ nanostructures towards the OER characterization were performed in 1.0 M KOH electrolytic solution using a three electrode cell set up. The use of 5mg of $NiCo_2O_4$ nanostructures in 2.5mL of deionized water and 50µL of 5% Nafion solution was mixed and sonicated in the ultrasonic bath for 20 min, and then homogenous

catalyst slurry was obtained. Three electrodes were consisted on Hg/HgO electrode as the reference electrode, graphite rod as counter electrode, and glassy carbon electrode (GCE) as working electrode. The cleaning of GCE was performed with 3µm alumina paste and silicon paper followed by washing with deionized water. The diameter of GCE was 3mm and it was modified with 5µL (0.2mg mass) of each prepared material. The electrochemical measurements were performed with linear sweep voltammetry (LSV) at 2mV/s. Electrochemical impedance spectroscopy was used to evaluate charge transport using frequency range of 100kHz to 1Hz at amplitude of 5mV and OER onset potential. Electrochemical active surface area (ECSA) was estimated from cyclic voltammetry curves at various scan rates using non-faradic region. The durability test was done with chronopotentiometry at 20 m.Acm$^{-2}$. All the experimental potentials recorded against Hg/HgO electrode as the reference electrode are converted to reversible hydrogen electrode (RHE) using Nernst equation. Tafel equation was used to study OER kinetics through estimation of Tafel slopes for the different $NiCo_2O_4$ nanostructures. All the measurements were performed at standard conditions.

### 2.3. Supercapacitor Applications

Supercapacitor application of as prepared $NiCo_2O_4$ nanostructures was investigated by three electrode and two electrode configurations in 3M KOH aqueous solution. The same type of reference and counter electrodes were used during supercapacitor characterization. The chronopotentiomerty was used for the recording of galvanostatic charge-discharge (GCD) curves and they were used to calculate the specific capacitance Cs (Fg$^{-1}$). The supercapacitor calculations were done with respect to specific capacitance, energy density and power density using three electrode configurations through reported work [59]. Following mathematical equations were used for this purpose:

$$C_s = \frac{I \times \Delta t}{m \times \Delta V} \quad (1)$$

Here Cs is specific capacitance, I current, $\Delta t$ discharge time, $\Delta V$ potential window, m is loading mass of electrode material

For the calculation of energy density under given equation was used [59]:

$$\mathrm{E_d} = \frac{\mathrm{C_s} \times (\Delta \mathrm{V}^2)}{2} \quad (2)$$

$E_d$ energy density, $C_s$ specific capacitance, $\Delta V^2$ change in potential

The power density was estimated by following equation [60]:

$$P_d = \frac{E}{\Delta t} \quad (3)$$

$P_d$ power density, E energy and $\Delta t$ discharge time

Asymmetric supercapacitor device was further designed using two electrode configuration consisting $NiCo_2O_4$ nanostructures (sample-2) as positive electrode and activated carbon (AC) was negative electrode in 3M KOH electrolytic solution. For the development of negative electrode, 20mg of AC was dissolved into 3mL of absolute ethanol and 1mL of deionized water with ratio of (3:1) using 150µL of 5% Nafion solution. Then, a homogenous mixture was obtained with sonication for 30min and it was drop casted onto the cleaned GCE and dried in vacuum. The $NiCo_2O_4$ nanostructures (sample-2) ink was used on other GCE electrode and dried in vacuum and used as positive electrode and the asymmetric supercapacitor was represented by $NiCo_2O_4$ NP//AC ASC. For the balancing of voltammetric charges (Q) of $NiCo_2O_4$ NP (Sample 2) and AC, the loaded mass of each electrode system was achieved on the basis of Q+ = Q– through equation [60-62]:

$$m+ m- = Cs- \Delta V- Cs+\Delta V+ \quad (4)$$

Here: m±, Cs±, and ΔV± shows the mass, specific capacitance, and potential range of $NiCo_2O_4$ NP (Sample 2) (+) and AC (−) electrodes, respectively. The estimated mass for m+/m− was around 0.17mg in $NiCo_2O_4$ NP//AC ASC. The use of total mass (M) for the calculation of specific capacitance (Cs, $Fg^{-1}$), energy density (E, $Wh.kg^{-1}$), and power density (P, $W.kg^{-1}$) was followed.

The calculations in terms of specific capacitance, energy density and powder density using two electrode systems were done according to the published work [63].

$$C_s = \frac{4 \times I \times \Delta t}{m \times \Delta V} \quad (5)$$

Where in Cs specific capacitance, I current, discharge time $\Delta t$, potential window ΔV, loading mass 'm'.

Energy density was calculated give below [63]:

$$E_d = \frac{C_s \times (\Delta V^2)}{7.2} \quad (6)$$

$E_d$ is energy density, specific capacitance $C_s$, potential change $\Delta V^2$

Moreover the power density of two electrodes was calculated by [63].

$$P_d = \frac{C_s \times 3600}{\Delta t} \quad (7)$$

$P_d$ power density, specific capacitance $C_s$, discharge time $\Delta V^2$

## 3. Results and discussion

### 3.1. Structural and crystalline characterization of $NiCo_2O_4$ nanostructures prepared with grapefruit juice

The SEM was used to observe the morphological aspects of the as-prepared $NiCo_2O_4$ nanostructures as shown in Figure1. The pure $NiCo_2O_4$ nanostructures exhibit the nanorods like morphology with interconnected network. The dimension of pure $NiCo_2O_4$ nanostructures would be around 200 to 300 nm with a length of few microns as shown in Figure 1a. The use of grapefruit juice has completely transformed the morphology of $NiCo_2O_4$ nanostructures from nanorods to short range nanoparticles as shown in Figures1b and 1c. The use of 1mL and 2mL of grape juice has shown almost same effect on the morphology and the associated morphology is like a short range nanoparticles with a size of 50-100 nm. The SEM observations suggest that the presence of wide range of functional hydroxyl and oxygenated groups from different chemical components of grape juice have played a dominant role to transform the catalyst morphology. These phytochemicals have tendency of reducing, capping and stabilizing agent, therefore they played a vital role to control the size and shape of $NiCo_2O_4$ material. Additionally, the grapefruit juice addition to growth solution results the change in the pH of solution towards acidic nature and consequently etching effect was expected which turned the 1D nanorod like morphology into compact 0D nanoparticles and modified the surface of as prepared $NiCo_2O_4$ nanostructures. Not

only the morphology transformation is caused by the use of grapefruit juice, but it has also added defects to the structure and modified the surface of $NiCo_2O_4$ nanostructures, consequently such favorable environment would be useful for the surface reason like OER. The crystal arrays were also studied by the XRD and the measured diffraction patterns are enclosed in Figure 1d. The preferred orientation of crystal growth can be seen along the (400) crystal planes followed by the (620) planes and the intensity of these planes is increasing with the increase in the amount of grapefruit. This scenario has significantly introduced the exposure of different crystal facets which could play useful role towards the water catalysis. However, the pure $NiCo_2O_4$ nanostructures have preferred crystal growth orientation among the (311) which could not be effective for efficient OER process; hence a limited catalytic activity was shown. The XRD results highlights that the crystal growth direction is also very essential parameter to evaluate the catalytic activity of newly developed electro catalyst for OER process. The other reflections for pure sample were 111, 220, 222, 422, 511, 531, 442, 533, and 622, however in case of grapefruit assisted $NiCo_2O_4$ nanostructures, some of the patterns were disappeared indicating that the reducing agents have either inhibited the crystal orientation or limited the growth along those crystal planes for the samples-1 and sample-2. Moreover, all the diffraction patterns of $NiCo_2O_4$ nanostructures well matched with the reference (card no: 01-080-1542). The XRD study has verified that the $NiCo_2O_4$ nanostructures prepared with grapefruit juice are only characterized by a spinel phase without any impurity.

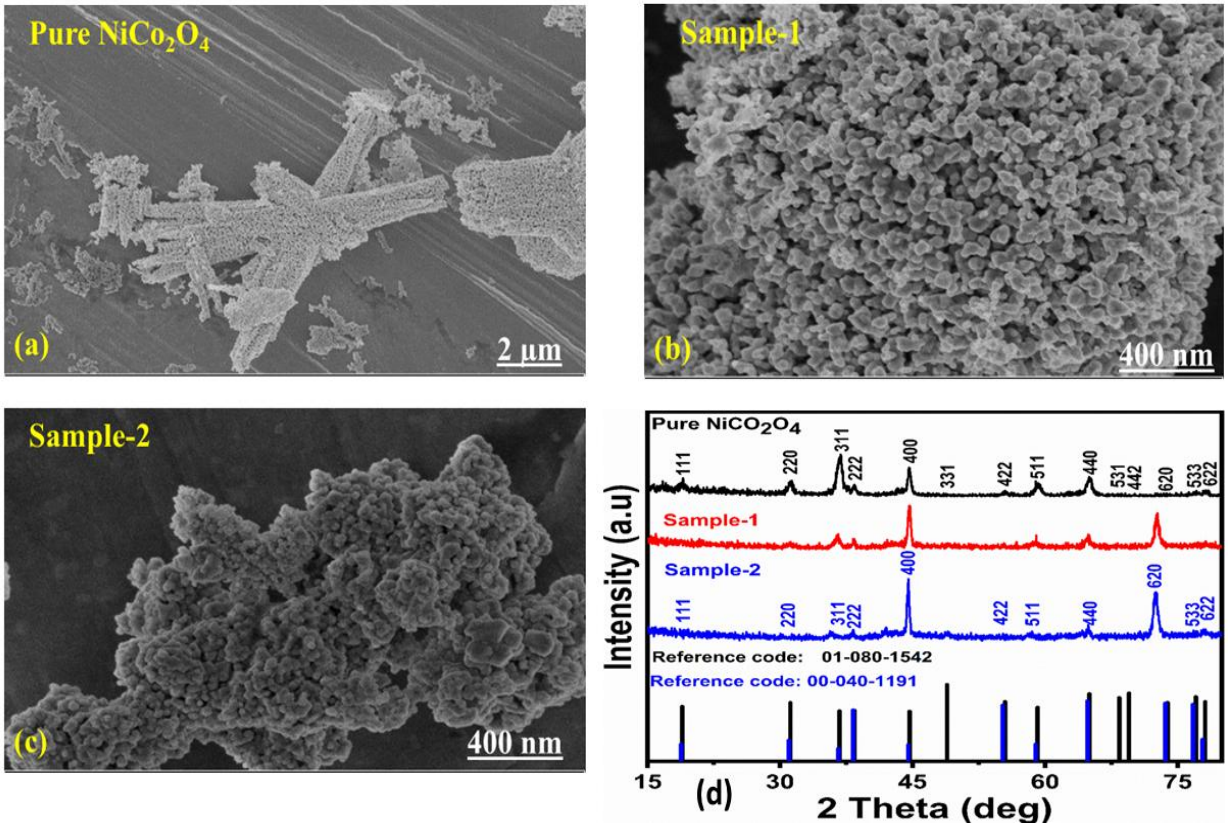


253 **Figure 1:** Typical SEM images of (a) pure $NiCo_2O_4$ nanostructures, (b,c) $NiCo_2O_4$
254 nanostructures with the use of 1 mL (sample-1) and 2mL (sample-2) of grapefruit juice, (d) XRD
255 diffraction patterns of $NiCo_2O_4$ nanostructures prepared with and without grapefruit juice.

256

257

258

259

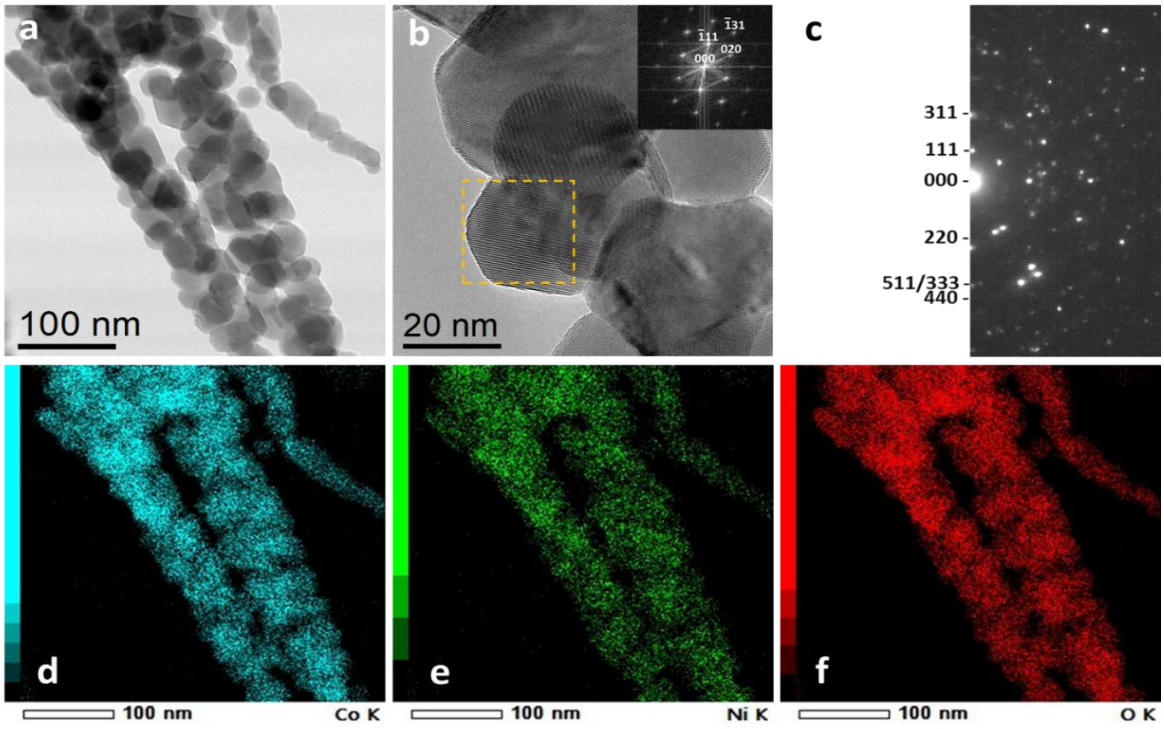


**Figure 2:** STEM Bright Field (BF) (a) and HRTEM (b) micrographs with corresponding Fast Fourier Transform (FFT) (insert of b) of pure $NiCo_2O_4$, SAED pattern of pure $NiCo_2O_4$ (c), and corresponding X-maps of cobalt (d), nickel (e) and oxygen (f).

High resolution transmission electron microscopy (HRTEM), selected area electron diffraction (SAED) and scanning transmission electron microscopy (STEM) coupled with energy dispersive X-ray spectroscopy (EDXS) experiments were performed on pristine and $NiCo_2O_4$ grown with grapefruit juice to determine their morphologies, their crystallographic structures and their chemical compositions. The pristine $NiCo_2O_4$ exhibits 1D nanorod-like morphology as seen on STEM BF micrograph (Figure 1a) in agreement with SEM. These nanorods are composed of pure $NiCo_2O_4$ nanoparticles as determined by EDXS (Figures-1d-f) and their diameter varies between 20 and 80 nanometers. SAED pattern presents rings at 4.7, 2.9 and 2.4Å (Figure 1c) confirming the Fd-3m cubic structure of $NiCo_2O_4$ (a = 8.1Å).

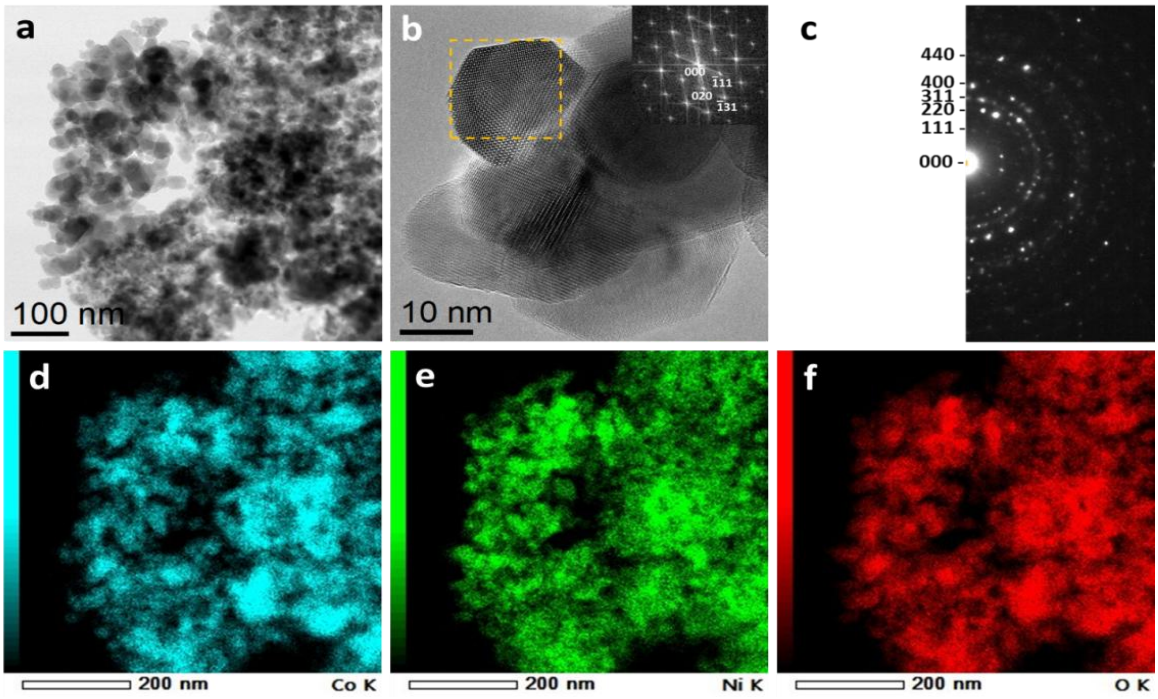


**Figure 3:** STEM Bright Field (BF) micrograph of $NiCo_2O_4$ grown with grapefruit (a), HRTEM micrograph of $NiCo_2O_4$ grown with grapefruit with corresponding Fast Fourier Transform (FFT) of one nanoparticle (yellow dashed square) (insert of b), SAED pattern of $NiCo_2O_4$ grown with grapefruit (c), and corresponding X-maps of cobalt (d), nickel (e) and oxygen (f).

Contrarily to pure $NiCo_2O_4$, $NiCo_2O_4$ grown with grapefruit juice sample presents aggregates of 0D nanoparticles with a diameter ranging from 10 to 50nm (Figures 3a and 3b). STEM-EDXS revealed that these nanoparticles are mainly composed of Co, Ni and O (Figures-3d-f). Additionally, SAED observations confirmed the Fd-3m cubic phase of $NiCo_2O_4$ nanostructures grown with grapefruit juice (Figure 3c), as supported by XRD analysis. TEM / STEM experiments highlighted that the main difference between both samples is clearly the nanorod-like morphology of pristine $NiCo_2O_4$, while $NiCo_2O_4$ grown with grapefruit juice exhibits aggregates of little, smaller nanoparticles. These observations evidence the impact of grapefruit in the morphology transformation, especially regarding the size of the grown $NiCo_2O_4$ nanoparticles. The results confirm the purity, excellent crystalline quality and controlled size of the prepared catalyst showing high accessible surface which is expected to have significant positive effect on water splitting at low energy demand.

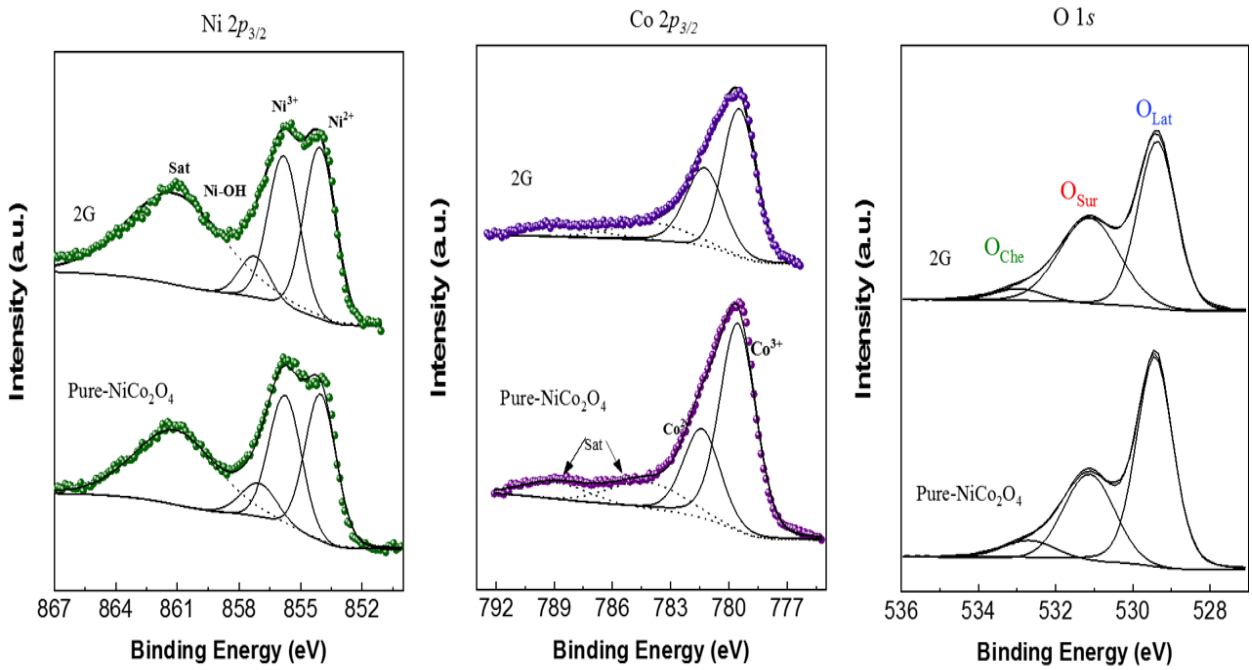


**Figure 4:** Ni $2p_{3/2}$, Co $2p_{3/2}$ and O 1*s* spectra of pure $NiCo_2O_4$ and grapefruit juice assisted $NiCo_2O_4$ nanostructures (2mL of grapefruit juice, 2G).

XPS analysis was carried out to find the surface information in terms of chemical states and composition on the surface. Figure 4 shows the corresponding Ni $2p_{3/2}$, Co $2p_{3/2}$ and O 1*s* signals at the core level of pure and grapefruit assisted $NiCo_2O_4$ structures. The Co $2p_{3/2}$ photoemission signal of pristine $NiCo_2O_4$ was decomposed in four contributions at 779.5, 781.4, 784.2 and 788.93eV and the obtained results are in good agreement with our previous studies [64-66] due to $Co^{3+}$, $Co^{2+}$, and two shake-up satellites, respectively. The Ni $2p_{3/2}$ signal, after decomposition, showed four contributions at 854.0, 855.7, 857.0 and 861.1eV due to $Ni^{2+}$, $Ni^{3+}$, $Ni(OH)_2$ and a satellite, respectively, according to literature data [67]. $NiCo_2O_4$ sample prepared with grapefruit juice showed a similar spectrum with the same contribution. No major changes in the BE were noticed. The main difference between both samples was the $Co^{2+}/Co^{3+}$ ratios. The pristine $NiCo_2O_4$ sample showed a $Ni^{2+}/Ni^{3+}$ ratio of 1.13 and a $Co^{2+}/Co^{3+}$ ratio of 0.44. These ratios were 1.15 and 0.66, respectively, for grapefruit derived sample, suggesting high amount of $Ni^{2+}$ and $Co^{2+}$ on the surface of $NiCo_2O_4$. XPS characterization has shown that the pristine and grapefruit $NiCo_2O_4$ samples showed mixed oxidation states, suggesting the typical spinel structure features of nickel-cobalt bimetallic oxides in good agreement with a previous study [68]. Moreover, the O1*s* core level signal showed three main peaks located at 529.4eV ($O_{Lat}$),

531.1eV ($O_{Surf}$) and 532.7eV ($O_{Chem}$). In both samples the peak at 529.4eV is distinctive of metal–oxygen chemical bonds. The peaks at around 531.1eV and 532.7eV in both materials are showing the surface defects and the impurities as shown in Figure 4. The peaks 531.1eV is mainly associated to oxygen vacancies and that at 532.7eV is connected to the chemisorbed oxygen [69]. The $O_{Surf}$ /$O_{Lat}$ ratio changed from 0.52 to 0.79 from pure to grapefruit juice derived nanostructure, *i.e.* the later contains a greater proportion of surface vacancies.

### 3.2. Half-cell OER characterization on various nanostructured $NiCo_2O_4$ samples

The performance evaluation of various $NiCo_2O_4$ samples prepared with the use of different juices of grapefruit was studied for OER activity in 1.0 M KOH electrolytic solution using three electrode electrochemical cell configurations like graphite rod as counter electrode, calomel (Hg/HgO) as reference electrode and glassy carbon electrode (GCE) modified with various $NiCo_2O_4$ samples as working electrode. A fixed mass of 5µL with a mass of 0.2 mg of various $NiCo_2O_4$ samples prepared the juice of grapefruit was deposited onto GCE and preliminary OER performance was evaluated using linear sweep voltammetry (LSV) as shown in Figure 5a. The bare GCE was also characterized for OER in contrast to the newly prepared $NiCo_2O_4$ samples and a relatively poor OER activity was observed as shown in Figure 4a. The overpotential against reversible hydrogen electrode (RHE) at 10 $m.Acm^{-2}$ was estimated for various $NiCo_2O_4$ samples like sample-1, sample-2 and pure $NiCo_2O_4$ with values of 290 mV, 260 mV and 300 mV, respectively. From these overpotential values, it is obvious that pure $NiCo_2O_4$ sample has relatively poor OER activity, compare to sample-1 and sample-2 suggesting that grapefruit juice has capability to tune the OER activity of $NiCo_2O_4$ material due to the presence of wide range of reducing and surface modifying agents in the grapefruit juice. The $NiCo_2O_4$ samples prepared with 1mL and 2mL of grapefruit juice have superior OER activities and the sample-2 has the highest OER activity with low overpotential of 260 mV. However, we have also noticed that further addition of grapefruit juice has reduced the OER activity; hence we did not provide the results of OER polarization curves. The enhanced electrochemical performance of $NiCo_2O_4$ sample prepared with 2 mL of grapefruit juice could be attributed to different type of phytochemicals having properties like reducing, capping and stabilizing agents which played a vital role during the growth process to control the morphology and size of nanostructured material. The results of well controlled size, shape, defects in the crystal structure and the surface oxygen vacancies obtained through SEM, TEM, XRD, and XPS were the factors to improve the electrochemical performance of $NiCo_2O_4$ material prepared ith 2 mL of grapefruit

juice. Additionally, the enhanced performance of $NiCo_2O_4$ sample prepared with 2mL of grapefruit juice could be associated to high amount of $Ni^{2+}$ r and $Co^{2+}$ on the surface of $NiCo_2O_4$. The OER kinetics was further illustrated from linear region of LSV OER polarization curves using Tafel analysis as shown in Figure 5b. The corresponding Tafel plots revealed a Tafel slopes for the sample-1, sample-2 and pure $NiCo_2O_4$ samples as 99mV.dec$^{-1}$, 95mV.dec$^{-1}$ and 104mV.dec$^{-1}$ respectively. The relatively low Tafel value for the sample-2 confirms that the OER kinetics is more favorable and it is directly connected to the surface morphology and rich surface active sites, hence it is characterized by low energy barrier as supported by the low overpotential of 260 mV. Furthermore, we have investigated the stability of $NiCo_2O_4$ sample-2 using LSV curves after 40h operation of durability experiment as shown in Figure 5c. The stability of $NiCo_2O_4$ sample-2 is highly preserved without any loss of current density, onset potential and overpotential and it highly strengthens the obtained results of durability measurements. The challenges in the development of efficient nonprecious electro catalysts for OER is the issue of durability for long term applications and have studied the stability of $NiCo_2O_4$ sample-2 using chronopotentiometry at fixed current density of 20 mA.cm$^{-1}$ as shown in Figure 5d. The stability of sample-2 is well maintained after 40h of continuous operation revealing that a negligible overpotential loss. The presented approach of using grapefruit juice to enhance the durability of $NiCo_2O_4$ sample based electrocatalyst could be connected to the stabilization of surface features by wide range of unique chemical compounds present in the grapefruit juice. We do also believe that future studies are needed to understand the role of each component of grapefruit juice to drive the OER activity at low overpotential and it can further help us to develop new generation of electrocatalysts in the near future, however in the proposed study we wanted to propose an alternative green and natural source of raw material to improve the catalytic properties of $NiCo_2O_4$ sample. Based on above highly enhanced and stable OER characterizaton of $NiCo_2O_4$ sample-2, Therefore, the presented study offers an alternative approach for the scale up synthesis of $NiCo_2O_4$ nanostructures for efficient OER activity and large scale applications.

To support electrochemical OER characterization, the charge transfer information at the interface about the OER reaction kinetics was evaluated for various $NiCo_2O_4$ samples using electrochemical impedance spectroscopy (EIS) as shown in Figure 5. The presentation of EIS is shown in Figure 5 e as Nyquist plots and Figure 5f as Bode plots. Figures 5f enable to show the information about the gain and phase aspects through various sweeping frequency, however the

charge transport at the interface could be seen from Figure-5e for different $NiCo_2O_4$ samples. The charge transfer resistance values of pure $NiCo_2O_4$ sample and grapefruit juice assisted $NiCo_2O_4$ (samples-1 and 2) are in the order 350Ω, 220Ω and 80Ω respectively. $NiCo_2O_4$ sample-2 is associated with faster charge transfer at the interface of electrode and electrolyte there by fosters the OER kinetics. The calculated charge transfer resistance and double capacitance values are given in Supplementary Table-S1. Moreover, we have studied the electrochemical active surface area (ECSA) through non-faradic region of cyclic voltammetry curves at various scan rates as shown in Supplementary (S1). The ECSA is directly connected to the double-layer capacitance (Cdl) of electrocatalyst material [70] which is used an indicator the quantification of actives sites involved in the OER reaction. From the CV curves, the value of Cdl could be collected by extracting the difference of current densities of anodic and cathodic non-faradic regions ($\Delta j = j_a - j_c$) at 1.10V versus RHE against the scan rate [71]. The corresponding slope of linear plotting divided by 2 gives the value of Cdl and the ECSA can be estimated by using a mathematical relation as ECSA: $C_{dl}/C_s$. Each material has its constant $C_s$ value depending on the nature electrode material surface which is reported value of 40mF.cm$^{-2}$ by previous work in 1.0M KOH [72]. The calculated ECSA values for various $NiCo_2O_4$ samples including pure $NiCo_2O_4$, $NiCo_2O_4$ sample-1 and $NiCo_2O_4$ sample-2 are 5.2μF.cm$^{-2}$, 7.6μF.cm$^{-2}$ and 18.1μF.cm$^{-2}$, respectively. The highest ECSA value of $NiCo_2O_4$ sample-2 verifies that it possesses many active sites utilized during OER reaction, leading to superior OER performance. Furthermore, the intrinsic activities of as prepared $NiCo_2O_4$ samples including pure $NiCo_2O_4$, $NiCo_2O_4$ sample-1 and $NiCo_2O_4$ sample-2 were evaluated using the normalization of their LSV curves with ECSA data as shown in as shown in Supplementary (S2). It was found that the enhanced electrochemical activity was connected with the increased surface area and related properties of $NiCo_2O_4$. The normalization of LSV curves of pure $NiCo_2O_4$, $NiCo_2O_4$ sample-1 and $NiCo_2O_4$ sample-2 with ECSA has been in good agreement with the previous work [73]. Moreover, low charge transfer resistance and high amount of ECSA of $NiCo_2O_4$ sample prepared with 2 mL of grapefruit juice also became the reasons for the enhanced electrochemical activity of as prepared material.

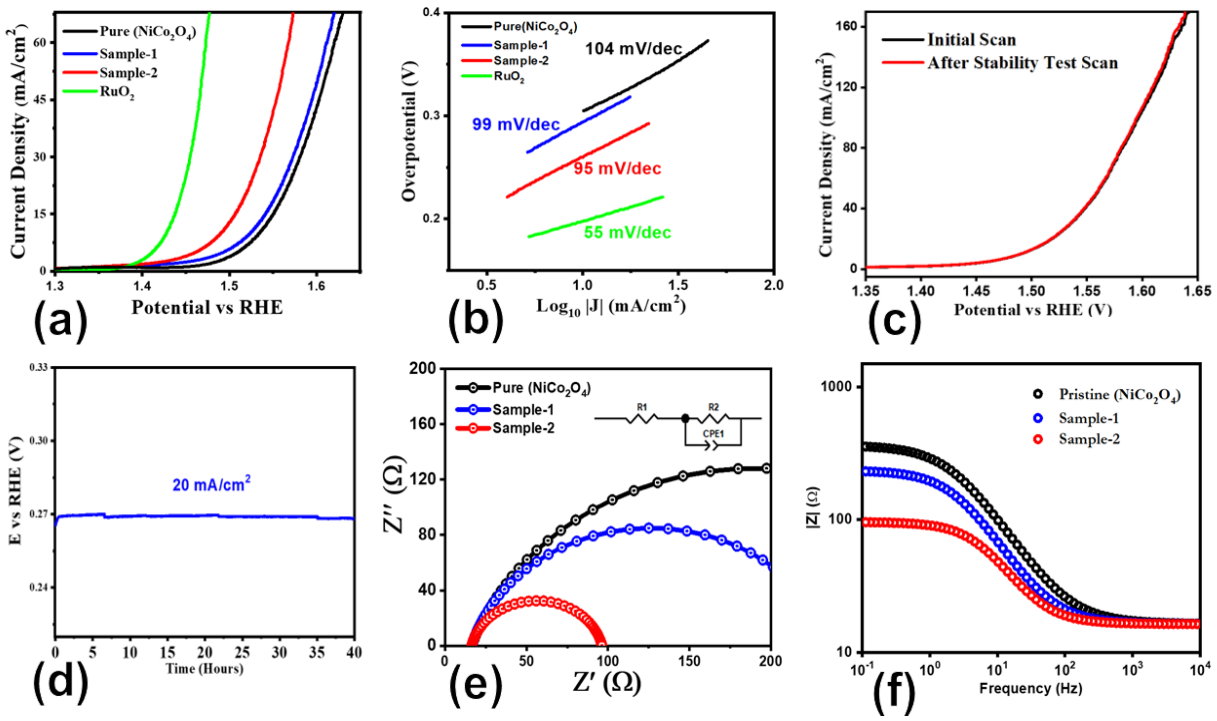


**Figure 5:** (a) LSV polarization curves at 2mV/s for pristine $NiCo_2O_4$ nanostructure, sample-1 sample-2 and $RuO_2$ in 1.0M KOH aqueous electrolytic solution, (b) Corresponding Tafel analysis, (c) stability of sample-2, (d) durability for 40 hours at 20mAcm$^{-2}$, (e) EIS Nyquist plots of pristine $NiCo_2O_4$ nanostructure, sample-1 sample-2 for frequency range of 100000 kHz to 0.1Hz at an amplitude of 10mV and onset potential of OER, inset shows the fitted equivalent circuit (f) Corresponded Bode Plots from same EIS.

### 3.2.Supercapacitor Investigations

Three electrode systems were used to evaluate the supercapacitor potential of various samples of $NiCo_2O_4$ nanostructures using CV and galvanostatic charge-discharge measurements as shown in Figure 6. Interestingly, CV curves of three $NiCo_2O_4$ samples at various scan rates ranging from 10 to 60mVs$^{-1}$, indicating typical pair of redox peaks for the potential range from 0 to 0.5V (vs. Hg/HgO) as shown in Figure 6(a-c). However, in case of pure $NiCo_2O_4$ nanostructures the redox behavior is limited and verifying the poor charge storage capacity with the material. But for the $NiCo_2O_4$ nanostructures (sample-1 and sample-2) prepared with grapefruit juice are well characterized by the typical redox peaks suggesting an excellent charge storage phenomenon within these two nanostructured samples of $NiCo_2O_4$ due to the dynamic aspects of Faradic mechanisms and they have distinctive battery type material properties. The redox process of

$NiCo_2O_4$ nanostructures was observed through the reversible Faradic redox reactions of $Co^{2+}/Co^{3+}$, $Ni^{2+}/Ni^{3+}$, and $Co^{3+}/Co^{4+}$ through the reported mechanism [18]:

$$NiCo_2O_4 + OH^- + H_2O \leftrightarrow NiOOH + 2CoOOH + e^- \quad (8)$$

$$CoOOH + OH^- \leftrightarrow CoO_2 + H_2O + e^- \quad (9)$$

On the applied higher scan rate, the cathodic peaks shifted slightly to lower potentials whereas the anodic peaks shifted to the opposite direction and it could be attributed to deficient incorporation of OH- into the center of nanostructured $NiCo_2O_4$ samples. The centered area of $NiCo_2O_4$ nanostructures (sample-2) is higher than (sample-1) and pure $NiCo_2O_4$ nanostructures at a scan rate $40mVs^{-1}$, indicating the specific capacitance of sample-2 relatively higher than the sample-1 and pure $NiCo_2O_4$ nanostructures. For the potential range of 0 to 0.5V (vs. Hg/HgO), GCD curves Figure 6(d-f) were measured at various current densities of 0.8 to $0.94Ag^{-1}$ and their GCD curves were with certain difference from the conventional triangular shapes with significant outlook of well-defined plateaus of charge and discharge curves. From the GCD curves, it's obvious that the sample-2 of $NiCo_2O_4$ nanostructures has higher Faradic features as confirmed from the CV curves of sample-2 when the current density was about $0.8Ag^{-1}$. Furthermore, the GCD curves of $NiCo_2O_4$ nanostructures (sample-1, sample-2 and pure $NiCo_2O_4$ nanostructures revealed that the specific capacitance of sample-2 is larger than the sample-1 and pure $NiCo_2O_4$ nanostructures as shown in Figure 6(d-f). The using mathematical equation from [57], the calculated specific capacitance for the $NiCo_2O_4$ nanostructures (sample-1, 2 and pure $NiCo_2O_4$ nanostructures were in the order to 178.00, 367.59 and $124.28Fg^{-1}$ at a current density of $0.8Ag^{-1}$ as shown in Figure 7a, at a current density of $0.94Ag^{-1}$, the specific capacitance were found to be 30.21, 31.74 and $43.50Fg^{-1}$ for $NiCo_2O_4$ nanostructures (sample-1, 2 and pure $NiCo_2O_4$ nanostructures respectively, confirming that 91.4.36% specific capacitance was retained compare to 8.6% at a current density of $0.94Ag^{-1}$. The retention of specific capacitance by sample-2 is higher than the pure $NiCo_2O_4$ nanostructures and (sample-1). The cycling stability was also evaluated by 900 GCD cycles for the $NiCo_2O_4$ nanostructures (sample-1, 2 and pure $NiCo_2O_4$ nanostructures as shown in Figure-7b, again sample-2 has shown an excellent cycling durability and high retention of specific capacitance after 900 cycles of GCD at $0.8Ag^{-1}$, and it further strengthened the claims of using grape juice for improving the electrochemical properties of $NiCo_2O_4$ nanostructures due to the presence of wide range of phytochemical chemicals. Because of the activation of three $NiCo_2O_4$ nanostructures (sample-1, 2 and pure) during the

stability test the cations from $NiCo_2O_4$ lattice planes slowly penetrate out and the electrolyte significantly diffuse inside the crystal arrays of $NiCo_2O_4$ nanostructures [72]. The high retention of % specific capacitance of sample-2 is verified as shown in Figure 7b. Beside the cycling stability was used to calculate the columbic efficiency of 47%, 73% and 45% for sample-1, sample-2 and pure sample of $NiCo_2O_4$ as shown in Figure 7c. The corresponding energy density of sample-1 of 8.13Wh/kg, sample-2 of 9.64Wh/kg, and pure sample of $NiCo_2O_4$ of 3.79Wh/Kg at current density of $0.8Ag^{-1}$ are shown in Figure 7(d-f) respectively. The sample-2 has demonstrated enhanced energy density at very low applied current density, confirming its potential aspect for the development of practical energy storage device. From CV, GCD and EIS together by the swift charge transfer of electron and fast diffusion of ions kinetically were assigned to the enhanced he supercapacitor performance. For the better presentation the calculated values of specific capacitance (Cs), energy density, power density, % retention of specific capacitance, and columbic efficiency are given in Table-1.

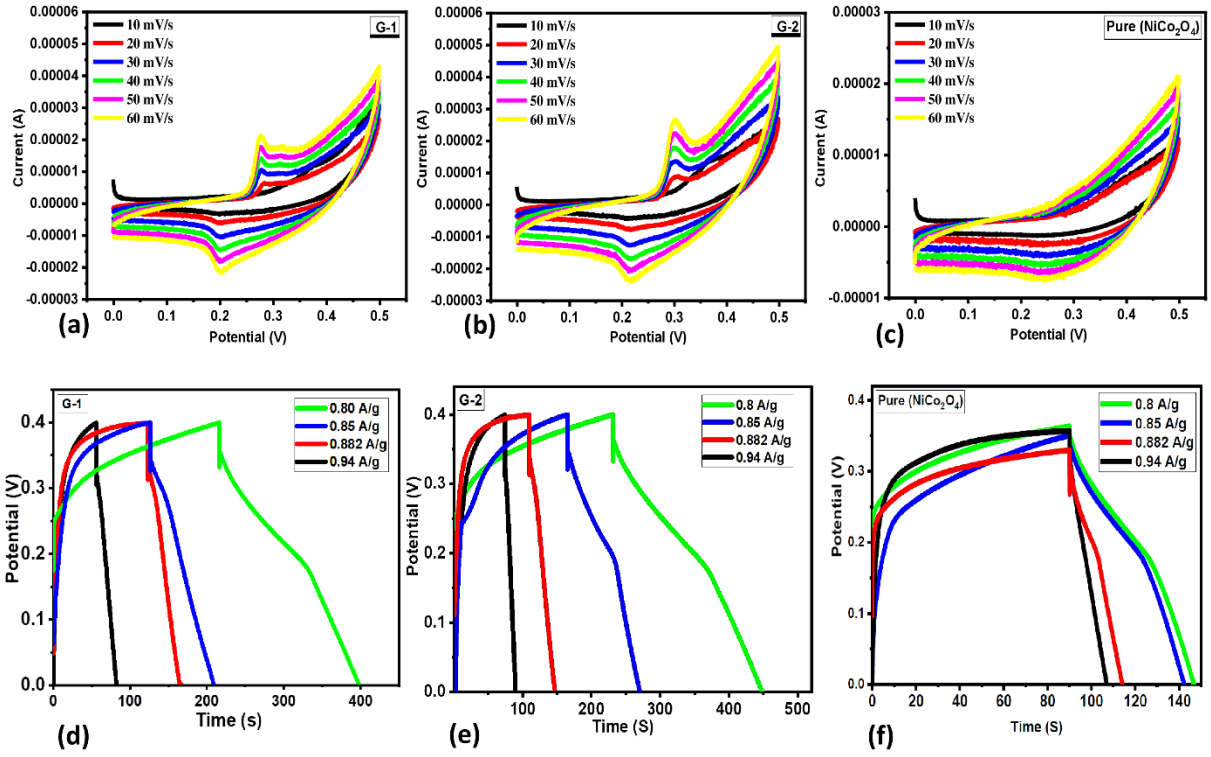

**Figure 6:** (a-c) CV curves at different scan rates for pristine $NiCo_2O_4$ nanostructure, sample-1 sample-2 in 3.0M KOH aqueous electrolytic solution, (d-f) Corresponding GCD curves at different current densities measured in 3.0M KOH solution.

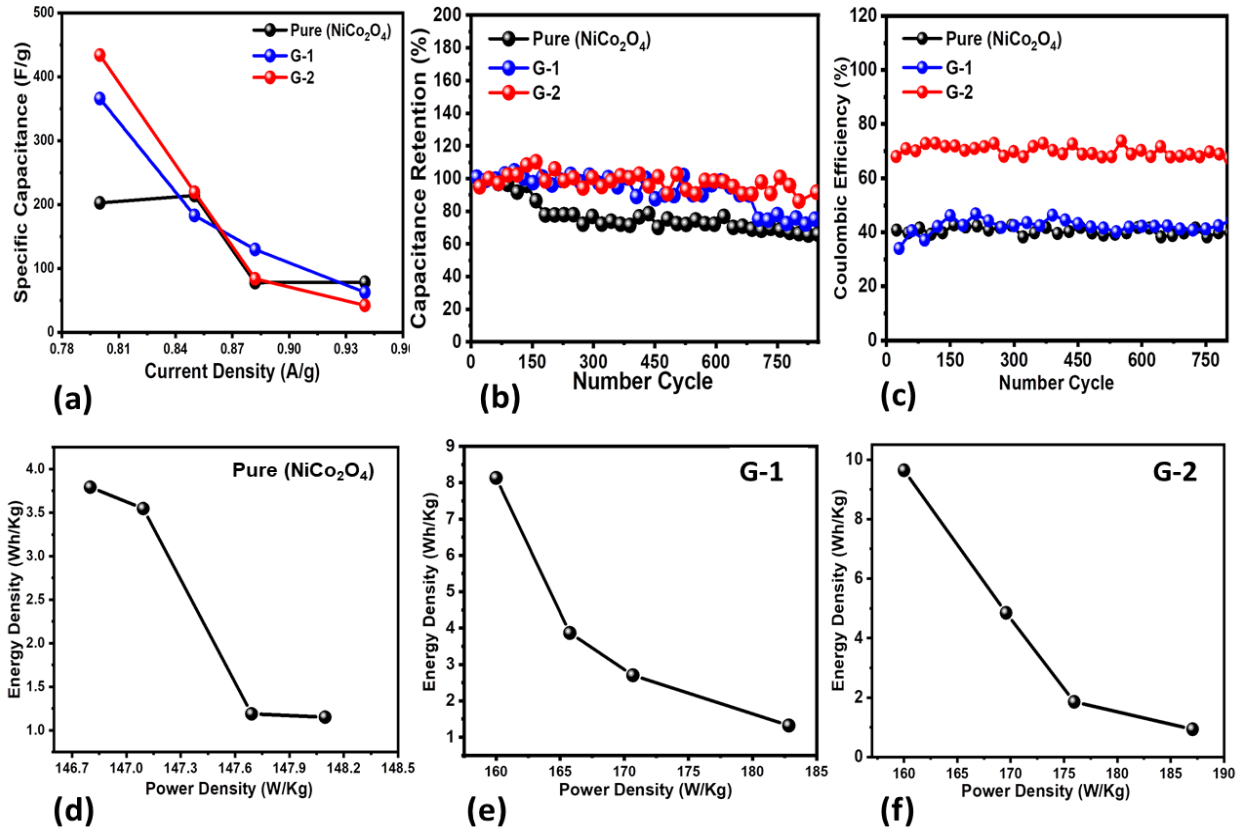


**Figure 7:** (a) specific capacitance of pristine $NiCo_2O_4$ nanostructure, sample 1(G1), sample 2(G2) from GCD curves, (b) percentage retention specific capacitance of pristine $NiCo_2O_4$ nanostructure, sample-1 (G1), sample-2 (G2) from 900 GCD repeatable cycles in 3.0M KOH for the illustration of cycling stability, (c) columbic efficiency of pristine $NiCo_2O_4$ nanostructure, sample-1 (G1) , sample-2 (G2) from 900 cycles stability of GCD curves in 3.0M KOH, (d-f) corresponding energy density of pristine $NiCo_2O_4$ nanostructure, sample-1 (G1), sample-2 (G2).

**Table 1:** The calculated various supercapacitor indicators for pristine $NiCo_2O_4$ nanostructure, sample-1 (G1) and sample-2 (G2).

| Samples | Current Density ($Ag^{-1}$) | Specific Capacitance ($Fg^{-1}$) | Energy Density (Wh $kg^{-1}$) | Power Density (W $kg^{-1}$) | Columbic Efficiency (%) | Capacitance Retention (%) |
|---|---|---|---|---|---|---|
| G-1 | 0.8 | 366.00 | 8.13 | 160.00 | 47% | 106-71% |
| | 0.85 | 183.08 | 3.87 | 165.75 | | |
| | 0.882 | 129.91 | 2.70 | 170.67 | | |
| | 0.94 | 62.83 | 1.32 | 182.83 | | |
| G-2 | 0.8 | 434.00 | 9.64 | 160.00 | 73% | 111-92% |
| | 0.85 | 219.42 | 4.85 | 169.58 | | |
| | 0.882 | 84.00 | 1.86 | 175.96 | | |
| | 0.94 | 42.51 | 0.94 | 187.06 | | |
| Pure NiCo2O4 | 0.8 | 202.72 | 3.79 | 146.80 | 45% | 100-65% |
| | 0.85 | 213.22 | 3.55 | 147.09 | | |
| | 0.882 | 76.38 | 1.19 | 147.69 | | |
| | 0.94 | 83.53 | 1.15 | 148.10 | | |

To study the promising features of $NiCo_2O_4$ nanostructures (sample2) towards practical aspects, an asymmetric supercapacitor represented as ($NiCo_2O_4$ NP//AC ASC) was configured using $NiCo_2O_4$ nanostructures (sample-2) was positive electrode and AC as negative electrode in a 3.0

M KOH electrolyte. As prepared AC exhibited a rectangular shape with the absence of redox peak and a significant specific capacitance of 50 $Fg^{-1}$ at 0.8$Ag^{-1}$ as shown supplementary (S3). For ASC device, the mass ratio of negative and positive electrode was estimated about 0.17mg. The loaded mass of negative electrode was about 5 mg. The $NiCo_2O_4$ nanostructures (sample 2) and AC CV curves were described in the Figure 8a and it was predicted to have potential range to 1.5V. The $NiCo_2O_4$ NP//AC ASC was characterized by CV curves and the overall capacitance was estimated from the double layer capacitance and battery type functionality of electrode. The CV curves with negligible shape alteration suggested the rapid charge-discharge properties of $NiCo_2O_4$ NP//AC ASC. The GCD curves of as developed asymmetric supercapacitor are enclosed in Figure 8b at different current densities from 0.8$Ag^{-1}$ to 0.94$Ag^{-1}$, whereas related supercapacitor calculations are show in Figure 8d. The specific capacitance of ASC device as found to be 1928.59$Fg^{-1}$, energy density of 41.77Wh.$kg^{-1}$ and power density of 631.84W/Kg at 0.8$Ag^{-1}$ as shown in Figure 8(d,e). The columbic efficiency of 42% and 100% capacitance retention was noticed during the 900 cycling durability test as shown in Figure 8e. The 100% retention of capacitance for 900 cycles confirms a significant rate stability of electrode material for long term energy storage applications as shown in Figure 8c. The measured asymmetric supercapacitor performance indicators are given in Table-2 for better understanding and visualization. Overall electrochemical performance of various samples like $RuO_2$, $NiCo_2O_4$ nanostructures (sample-1, 2 and pure) in terms of overpotential, Tafel slope values, specific capacitance and energy density are further clearly represented through bar graphs view as shown in supplementary (S4).

The performance evaluation was prepared $NiCo_2O_4$ NP//AC ASC device was compared with several recently reported works as given in Table-S2. It obvious that the presented ASC device has either superior or comparable performance in terms of specific capacitance, energy density, power density and columbic efficiency. Based on the overall an excellent performance of $NiCo_2O_4$ nanostructures (sample-2) towards OER and SC applications which could contributed from large surface area owing to short range nanoparticles, high electrical conductivity, fast electron transfer, strong contact of nanoparticles with electrode to bioactive mimic effect, favorable interface chemistry, small packets of nanoparticles allowed the frequent electrode to electrolyte communication, the bioactive mimic effect minimized the volume changes, hence a realization of mechanical durability, and high structure integrity of the electrode material during the cycling measurements. Furthermore, the OER performance of as prepared $NiCo_2O_4$

nanostructures (sample-2) was compared with recently reported electrocatalyst as given Supplementary Table-S3. It is obvious under the similar conditions of alkaline electrolyte, the energy demand for OER was found lower for the $NiCo_2O_4$ nanostructures (sample-2) compared to the exiting electrocatalysts, hence it can be capitalized as an alternative material for the energy conversion applications. Generally, energy storage mechanism in alkaline conditions has been described as:

The physicochemical properties of $NiCo_2O_4$ are highly tuned by the presence of nickel atom due to its similar size to that of cobalt atom, hence obviously crystal structure is changed which further causes the defects. These defects may play unexpected role towards electrochemical activity of $NiCo_2O_4$ as shown in several reported works [74, 75]. The $NiCo_2O_4$ exhibits potential window in the range of 0 to 0.55 V in alkaline electrolyte conditions and its pseudo capacitance properties could be described through equation 8 and 9. The energy storage mechanism is presented in the Supplementary Scheme 3. It has been shown during the charging-discharging experiment onto the surface of $NiCo_2O_4$ electrode material, there is variation of oxidation states of $Co^{3+}/Co^{4+}$ along with the $Ni^{2+}/Ni^{3+}$, hereby the swift reversible Faradic processes take place [76, 77]. It has been found that the electrochemical redox potentials of $Ni^{2+}/Ni^{3+}$ and $Co^{3+}/Co^{4+}$ transition are very much close, consequently the redox peaks found to be closely merged [76, 77].

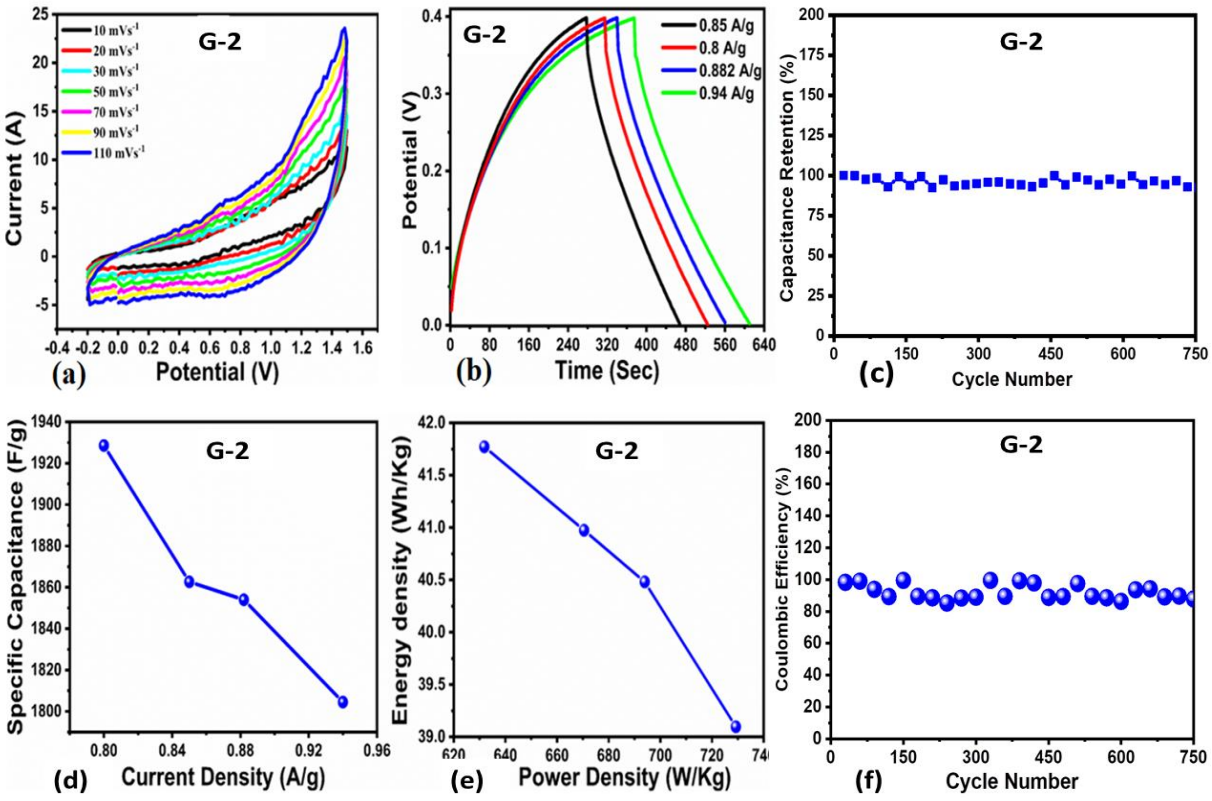


546

547 **Figure 8:** CV curves of sample-2 (G2) at different scan rates in 3.0M KOH, (b) GCD curves at
548 different current density for sample-2 (G2), (c) Cycling stability of sample-2 (G2) during 900
549 GCD repeatable cycles in 3.0M KOH , (d) specific capacitance of sample-2 (G2) from GCD
550 curves, (e) Energy density of sample-2 (G2), (f) Columbic efficiency during 900 repeatable GCD
551 cycles in 3.0M KOH

**Table 2:** Measured indicators for asymmetric supercapacitor using two electrode configurations for practical applications.

| Samples | Current Density ($Ag^{-1}$) | Specific Capacitance ($Fg^{-1}$) | Energy Density ($Wh\ kg^{-1}$) | Power Density (W/Kg) | Columbic Efficiency % | Capacitance Retention % |
|---|---|---|---|---|---|---|
| G-2 | 0.8 | 1928.59 | 41.77 | 631.84 | 100-81% | 100-93% ( 900 Cycles) |
| | 0.85 | 1896.55 | 40.97 | 670.48 | | |
| | 0.882 | 1883.27 | 40.48 | 693.96 | | |
| | 0.94 | 1870.79 | 39.09 | 729.25 | | |

## 4. Conclusions

In summary, a green approach was used to synthesize short range nanoparticles of $NiCo_2O_4$ with high surface vacancies, rich surface with $Ni^{2+}$ and $Co^{2+}$, large active sites and fast charge transport for the OER half-cell reaction. The grapefruit juice has a wide range of functional molecules, which can act as either reducing agents or surface modifying agents. Importantly, the 1D $NiCo_2O_4$ structure was successfully changed into 0D structure. The chemical components of the grapefruit juice have proved to be potential candidates to tune the electrochemical performance of $NiCo_2O_4$ nanostructures. The OER was evident to occur at markedly low overpotential of 260 mV at 10 $mA.cm^{-2}$ which is significantly improved performance from a low

cost and earth abundant material. The enhanced OER activity was strongly supported by the charge transfer at the interface and involvement of high active surface area during the process. Based on these results, we conclude that the grapefruit is a powerful natural source playing as reducing and surface modifying agents for tailoring the surface-based reactions at swift kinetics. Thus, it can be used as an alternative raw material for the development of new generation of electrocatalysts for energy conversion and storage systems.


## Acknowledgments

We extend our sincere appreciations to Researchers Supporting Project number (RSP2023R79), King Saud University, Riyadh, Saudi Arabia, for partial funding of this work. We also would like to thank the platform "Microscopies, Microprobes and Metallography (3M)" at the Institut Jean Lamour (IJL, Nancy, France) for TEM and SEM facilities.


## Conflict of Interest

Authors have no conflict of interest in the presented research work

## 5. References


[1] Huang W, Zheng D, Chen X, Shi L, Dai X, Chen Y, Jing X. Standard thermodynamic properties for the energy grade evaluation of fossil fuels and renewable fuels. Renewable Energy. 2020;147:2160-70.

[2] Centi G, Perathoner S. Chemistry and energy beyond fossil fuels. A perspective view on the role of syngas from waste sources. Catalysis Today. 2020;342:4-12.

[3] Duić N, Guzović Z, Kafarov V, Klemeš JJ, vad Mathiessen B, Yan J. Sustainable development of energy, water and environment systems. Applied Energy. 2013;101:3-5.

[4] Tolón-Becerra A, Lastra-Bravo X, Bienvenido-Bárcena F. Proposal for territorial distribution of the EU 2020 political renewable energy goal. Renewable Energy. 2011;36:2067-77.

[5] Suganthi L, Williams A. Renewable energy in India—a modelling study for 2020–2021. Energy policy. 2000;28:1095-109.

[6] Lowitzsch J, Hoicka CE, van Tulder FJ. Renewable energy communities under the 2019 European Clean Energy Package–Governance model for the energy clusters of the future?. Renewable and Sustainable Energy Reviews. 2020;122:109489.

[7] Qazi A, Hussain F, Rahim NA, Hardaker G, Alghazzawi D, Shaban K, Haruna K. Towards sustainable energy: a systematic review of renewable energy sources, technologies, and public opinions. IEEE access. 2019;7:63837-51.

[8] Dudin MN, Frolova EE, Protopopova OV, Mamedov O, Odintsov SV. Study of innovative technologies in the energy industry: nontraditional and renewable energy sources. Entrepreneurship and Sustainability Issues. 2019;6:1704.

[9] Zhou Y, Fan HJ. Progress and challenge of amorphous catalysts for electrochemical water splitting. ACS Materials Letters. 2020;3:136-47.

[10] Li L, Wang P, Shao Q, Huang X. Metallic nanostructures with low dimensionality for electrochemical water splitting. Chemical Society Reviews. 2020;49:3072-106.

[11] Ham K, Hong S, Kang S, Cho K, Lee J. Extensive active-site formation in trirutile CoSb2O6 by oxygen vacancy for oxygen evolution reaction in anion exchange membrane water splitting. ACS Energy Letters. 2021;6:364-70.

[12] Li C, Baek JB. Recent advances in noble metal (Pt, Ru, and Ir)-based electrocatalysts for efficient hydrogen evolution reaction. ACS omega. 2019;5:31-40.

[13] Reier T, Oezaslan M, Strasser P. Electrocatalytic oxygen evolution reaction (OER) on Ru, Ir, and Pt catalysts: a comparative study of nanoparticles and bulk materials. Acs Catalysis. 2012;2:1765-72.

[14] Wu ZP, Lu XF, Zang SQ, Lou XW. Non-noble-metal-based electrocatalysts toward the oxygen evolution reaction. Advanced Functional Materials. 2020;30:1910274.

[15] Zhu C, Wen D, Leubner S, Oschatz M, Liu W, Holzschuh M, Simon F, Kaskel S, Eychmüller A. Nickel cobalt oxide hollow nanosponges as advanced electrocatalysts for the oxygen evolution reaction. Chemical communications. 2015;51:7851-4.

[16] Jiang J, Zhang A, Li L, Ai L. Nickel–cobalt layered double hydroxide nanosheets as high-performance electrocatalyst for oxygen evolution reaction. Journal of Power Sources. 2015;278:445-51.

[17] Eftekhari A. Materials today energy. Mater. Today. 2017;5:37-57.

[18] Noor T, Yaqoob L, Iqbal N. Recent advances in electrocatalysis of oxygen evolution reaction using noble-metal, transition-metal, and carbon-based materials. ChemElectroChem. 2021;8:447-83.

[19] Moon GH, Yu M, Chan CK, Tüysüz H. Highly Active Cobalt-Based Electrocatalysts with Facile Incorporation of Dopants for the Oxygen Evolution Reaction. Angewandte Chemie. 2019;131:3529-33.

[20] Song F, Bai L, Moysiadou A, Lee S, Hu C, Liardet L, Hu X. Transition metal oxides as electrocatalysts for the oxygen evolution reaction in alkaline solutions: an application-inspired renaissance. Journal of the American Chemical Society. 2018;140:7748-59.

[21] di Lena F, Matyjaszewski K. Transition metal catalysts for controlled radical polymerization. Progress in Polymer Science. 2010;35:959-1021.

[22] Kinzel NW, Werlé C, Leitner W. Transition metal complexes as catalysts for the electroconversion of CO2: an organometallic perspective. Angewandte Chemie International Edition. 2021;60:11628-86.

[23] Sun H, Yan Z, Liu F, Xu W, Cheng F, Chen J. Self-supported transition-metal-based electrocatalysts for hydrogen and oxygen evolution. Advanced materials. 2020;32:1806326.

[24] Sivanantham A, Ganesan P, Shanmugam S. Hierarchical NiCo2S4 nanowire arrays supported on Ni foam: an efficient and durable bifunctional electrocatalyst for oxygen and hydrogen evolution reactions. Advanced Functional Materials. 2016;26:4661-72.

[25] Iqbal MF, Ashiq MN, Iqbal S, Bibi N, Parveen B. High specific capacitance and energy density of synthesized graphene oxide based hierarchical Al2S3 nanorambutan for supercapacitor applications. Electrochimica Acta. 2017;246:1097-103.

[26] Wang F, Wang X, Chang Z, Wu X, Liu X, Fu L, Zhu Y, Wu Y, Huang W. A quasi-solid-state sodium-ion capacitor with high energy density. Advanced Materials. 2015;27:6962-8.

[27] Wang F, Wu X, Yuan X, Liu Z, Zhang Y, Fu L, Zhu Y, Zhou Q, Wu Y, Huang W. Latest advances in supercapacitors: from new electrode materials to novel device designs. Chemical Society Reviews. 2017;46:6816-54.

[28] Chen X, Liu J, Yuan T, Zhang Z, Song C, Yang S, Gao X, Wang N, Cui L. Recent advances in earth-abundant first-row transition metal (Fe, Co and Ni)-based electrocatalysts for the oxygen evolution reaction. *Energy Mater* 2022;2:200028.

[29] Dai H, Zhou R, Zhang Z, Zhou J, Sun G. Design of manganese dioxide for supercapacitors and zinc-ion batteries: similarities and differences. *Energy Mater* 2022;2:200040.

[30] Li X, Walsh FC, Pletcher D. Nickel based electrocatalysts for oxygen evolution in high current density, alkaline water electrolysers. Physical Chemistry Chemical Physics. 2011;13:1162-7.

[31] Vij V, Sultan S, Harzandi AM, Meena A, Tiwari JN, Lee WG, Yoon T, Kim KS. Nickel-based electrocatalysts for energy-related applications: oxygen reduction, oxygen evolution, and hydrogen evolution reactions. Acs Catalysis. 2017;7:7196-225.

[32] Liu Y, Xu Q, Wang R, Zheng Y, Zhu L, Wang Z, Zheng W. Ionothermal synthesis of three-dimensional hierarchical Ni 3 Se 2 mesoporous nanosheet networks with enhanced performance for asymmetric supercapacitors. Journal of Materials Chemistry A. 2020;8:797-809.

[33] Zhang X, Lu W, Tian Y, Yang S, Zhang Q, Lei D, Zhao Y. Nanosheet-assembled NiCo-LDH hollow spheres as high-performance electrodes for supercapacitors. Journal of Colloid and Interface Science. 2022;606:1120-7.

[34] Kong D, Wang Y, Huang S, Hu J, Von Lim Y, Liu B, Fan S, Shi Y, Yang HY. 3D self-branched zinc-cobalt Oxide@ N-doped carbon hollow nanowall arrays for high-performance asymmetric supercapacitors and oxygen electrocatalysis. Energy Storage Materials. 2019;23:653-63.

[35] Wang A, Chen Y, Zheng Z, Wang H, Li X, Yang Z, Qiu R, Yan K. In situ N-doped carbon-coated mulberry-like cobalt manganese oxide boosting for visible light driving photocatalytic degradation of pharmaceutical pollutants. Chemical Engineering Journal. 2021;411:128497.

[36] Deshagani S, Maity D, Das A, Deepa M. NiMoO4@ NiMnCo2O4 Heterostructure: A Poly (3, 4-propylenedioxythiophene) Composite-Based Supercapacitor Powers an Electrochromic Device. ACS Applied Materials & Interfaces. 2021;13:34518-32.

[37] Liu L, Zhang H, Yang J, Mu Y, Wang Y. Self-assembled novel dandelion-like NiCo 2 O 4 microspheres@ nanomeshes with superior electrochemical performance for supercapacitors and lithium-ion batteries. Journal of Materials Chemistry A. 2015;3:22393-403.

[38] Fu H, Liu Y, Chen L, Shi Y, Kong W, Hou J, Yu F, Wei T, Wang H, Guo X. Designed formation of NiCo2O4 with different morphologies self-assembled from nanoparticles for asymmetric supercapacitors and electrocatalysts for oxygen evolution reaction. Electrochimica Acta. 2019;296:719-29.

[39] Liu T, Diao P. Nickel foam supported Cr-doped NiCo2O4/FeOOH nanoneedle arrays as a high-performance bifunctional electrocatalyst for overall water splitting. Nano Research. 2020;13:3299-309.

[40] Kumar L, Chauhan M, Boruah PK, Das MR, Hashmi SA, Deka S. Coral-shaped bifunctional NiCo2O4 nanostructure: a material for highly efficient electrochemical charge storage and electrocatalytic oxygen evolution reaction. ACS Applied Energy Materials. 2020;3:6793-804.

[41] Zhu Y, Ji X, Wu Z, Song W, Hou H, Wu Z, He X, Chen Q, Banks CE. Spinel NiCo2O4 for use as a high-performance supercapacitor electrode material: understanding of its electrochemical properties. Journal of Power Sources. 2014;267:888-900.

[42] Gao X, Zhang H, Li Q, Yu X, Hong Z, Zhang X, Liang C, Lin Z. Hierarchical NiCo2O4 hollow microcuboids as bifunctional electrocatalysts for overall water-splitting. Angewandte Chemie International Edition. 2016;55:6290-4.

[43] Mondal A, Maiti S, Singha K, Mahanty S, Panda AB. TiO 2-rGO nanocomposite hollow spheres: large scale synthesis and application as an efficient anode material for lithium-ion batteries. Journal of Materials Chemistry A. 2017;5:23853-62.

[44] Fang L, Jiang Z, Xu H, Liu L, Gu X, Wang Y. Crystal-plane engineering of NiCo2O4 electrocatalysts towards efficient overall water splitting. Journal of catalysis. 2018;357:238-46.

[45] Lv X, Zhu Y, Jiang H, Yang X, Liu Y, Su Y, Huang J, Yao Y, Li C. Hollow mesoporous NiCo 2 O 4 nanocages as efficient electrocatalysts for oxygen evolution reaction. Dalton Transactions. 2015;44:4148-54.

[46] Penniston KL, Nakada SY, Holmes RP, Assimos DG. Quantitative assessment of citric acid in lemon juice, lime juice, and commercially-available fruit juice products. Journal of Endourology. 2008;22:567-70.

[47] Kejík Z, Kaplánek R, Masařík M, Babula P, Matkowski A, Filipenský P, Veselá K, Gburek J, Sýkora D, Martásek P, Jakubek M. Iron complexes of flavonoids-antioxidant capacity and beyond. International Journal of Molecular Sciences. 2021;22:646.

[48] Panić M, Gunjević V, Cravotto G, Redovniković IR. Enabling technologies for the extraction of grape-pomace anthocyanins using natural deep eutectic solvents in up-to-half-litre batches extraction of grape-pomace anthocyanins using NADES. Food Chemistry. 2019;300:125185.

[49] Ballistreri G, Fabroni S, Romeo FV, Timpanaro N, Amenta M, Rapisarda P. Anthocyanins and other polyphenols in citrus genus: Biosynthesis, chemical profile, and biological activity. In Polyphenols in plants 2019:191-215.

[50] Akshaya KB, Varghese A, Sudhakar YN, George L. Electrocatalytic oxidation of morin on electrodeposited Ir-PEDOT nanograins. Food chemistry. 2019;270:78-85.

[51] Xue J, Liu J, Liu Y, Li H, Wang Y, Sun D, Wang W, Huang L, Tang J. Recent advances in synthetic methods and applications of Ag 2 S-based heterostructure photocatalysts. Journal of Materials Chemistry C. 2019;7:3988-4003.

[52] Yu J, He Q, Yang G, Zhou W, Shao Z, Ni M. Recent advances and prospective in ruthenium-based materials for electrochemical water splitting. Acs Catalysis. 2019;9:9973-10011.

[53] Russo D. Flavonoids and the structure-antioxidant activity relationship. J Pharmacogn Nat Prod. 2018;4:e109.

[54] Wang S, Feng T, Wang Y, Qiu Y. Recent Advances in Electrocarboxylation with CO2. Chemistry–An Asian Journal. 2022;17:e202200543.

[55] Chen LA, House L. An overview of the grapefruit market in the US: FE1095/FE1095, 05/2021. EDIS. 2021;2021:3-15.

[56] Brouzgou A, Gorbova E, Wang Y, Jing S, Seretis A, Liang Z, Tsiakaras P. Nitrogen-doped 3D hierarchical ordered mesoporous carbon supported palladium electrocatalyst for the simultaneous detection of ascorbic acid, dopamine, and glucose. Ionics. 2019;25:6061-70.

[57] Klimek-Szczykutowicz M, Szopa A, Ekiert H. Citrus limon (Lemon) phenomenon—a review of the chemistry, pharmacological properties, applications in the modern pharmaceutical, food, and cosmetics industries, and biotechnological studies. Plants. 2020;9:119.

[58] Uckoo RM, Jayaprakasha GK, Balasubramaniam VM, Patil BS. Grapefruit (Citrus paradisi Macfad) phytochemicals composition is modulated by household processing techniques. Journal of food science. 2012;77:C921-6.

[59] Jokar E, Shahrokhian S. Synthesis and characterization of NiCo2O4 nanorods for preparation of supercapacitor electrodes. Journal of Solid State Electrochemistry. 2015;19:269-74.

[60] Yan Y, Bao K, Liu T, Cao J, Feng J, Qi J. Minutes periodic wet chemistry engineering to turn bulk Co-Ni foam into hydroxide based nanosheets for efficient water decomposition. Chemical Engineering Journal. 2020;401:126092.

[61] Rashti A, Lu X, Dobson A, Hassani E, Feyzbar-Khalkhali-Nejad F, He K, Oh TS. Tuning MOF-derived Co3O4/NiCo2O4 nanostructures for high-performance energy storage. ACS Applied Energy Materials. 2021;4:1537-47.

[62] Gopi CV, Vinodh R, Sambasivam S, Obaidat IM, Kim HJ. Recent progress of advanced energy storage materials for flexible and wearable supercapacitor: From design and development to applications. Journal of energy storage. 2020;27:101035.

[63] Young C, Salunkhe RR, Alshehri SM, Ahamad T, Huang Z, Henzie J, Yamauchi Y. High energy density supercapacitors composed of nickel cobalt oxide nanosheets on nanoporous carbon nanoarchitectures. Journal of Materials Chemistry A. 2017;5:11834-9.

[64] Ibupoto ZH, Tahira A, Shah AA, Aftab U, Solangi MY, Leghari JA, Samoon AH, Bhatti AL, Bhatti MA, Mazzaro R, Morandi V. NiCo2O4 nanostructures loaded onto pencil graphite rod: An advanced composite material for oxygen evolution reaction. International Journal of Hydrogen Energy. 2022;47:6650-65.

[65] Bhatti AL, Tahira A, Gradone A, Mazzaro R, Morandi V, Abro MI, Nafady A, Qi K, Infantes-Molina A, Vomiero A, Ibupoto ZH. Nanostructured Co3O4 electrocatalyst for OER: the role of organic polyelectrolytes as soft templates. Electrochimica Acta. 2021;398:139338.

[66] Aftab U, Tahira A, Mazzaro R, Abro MI, Baloch MM, Willander M, Nur O, Yu C, Ibupoto ZH. The chemically reduced CuO–Co 3 O 4 composite as a highly efficient electrocatalyst for oxygen evolution reaction in alkaline media. Catalysis Science & Technology. 2019;9:6274-84.

[67] Wei Z, Guo J, Qu M, Guo Z, Zhang H. Honeycombed-like nanosheet array composite NiCo2O4/rGO for efficient methanol electrooxidation and supercapacitors. Electrochimica Acta. 2020;362:137145.

[68] Laghari AJ, Aftab U, Tahira A, Shah AA, Gradone A, Solangi MY, Samo AH, Abro MI, wasim Akhtar M, Mazzaro R, Morandi V. MgO as promoter for electrocatalytic activities of Co3O4–MgO composite via abundant oxygen vacancies and Co2+ ions towards oxygen evolution reaction. International Journal of Hydrogen Energy. 2022.

[69] Zhang G, Qin Q, Luo W, Liu Y, Jin C, Hao J, Zhang J, Zheng W. A combination–decomposition method to synthesize two-dimensional metal sulfide–amine hybrid nanosheets: a highly efficient Fe-based water oxidation electrocatalyst. Chemical Communications. 2018;54:4617-20.

[70] Xu Q, Liu Y, Tian Z, Shi Y, Wang Z, Zheng W. Fabrication of heterogeneous interface and phosphorus doping in MoS2 for efficient hydrogen evolution in both acid and alkaline electrolytes. Electrochimica Acta. 2021;385:138429.

[71] Li W, Gao X, Xiong D, Wei F, Song WG, Xu J, Liu L. Hydrothermal synthesis of monolithic Co3Se4 nanowire electrodes for oxygen evolution and overall water splitting with high efficiency and extraordinary catalytic stability. Advanced Energy Materials. 2017;7:1602579.

[72] Zhang J, Feng H, Qin Q, Zhang G, Cui Y, Chai Z, Zheng W. Interior design of three-dimensional CuO ordered architectures with enhanced performance for supercapacitors. Journal of Materials Chemistry A. 2016;4:6357-67.

[73] Hangjuan R, Ying P, Charles C. S, Haiwei D. Assessment of electrocatalytic activity through the lens of three surface area normalization techniques. Journal of Materials Chemistry A. 2020;8:3154-3159.

[74] Liu X, Shi S, Xiong Q, Li L, Zhang Y, Tang H, Gu C, Wang X, Tu J. Hierarchical NiCo2O4@ NiCo2O4 core/shell nanoflake arrays as high-performance supercapacitor materials. ACS applied materials & interfaces. 2013; 17:8790-5.

[75] Chen Y, Qu B, Hu L, Xu Z, Li Q, Wang T. High-performance supercapacitor and lithium-ion battery based on 3D hierarchical NH 4 F-induced nickel cobaltate nanosheet–nanowire cluster arrays as self-supported electrodes. Nanoscale. 2013; 20: 9812-20.

[76] Haenen J, Visscher W, Barendrecht E. Characterization of NiCo2O4 electrodes for O2 evolution: Part I. Electrochemical characterization of freshly prepared NiCo2O4 electrodes. Journal of electroanalytical chemistry and interfacial electrochemistry. 1986; 2: 273-96.

[77] Rasiyah P, Tseung AC, Hibbert DB. A Mechanistic Study of Oxygen Evolution on NiCo2 O 4: I. Formation of Higher Oxides. Journal of the Electrochemical Society. 1982; 8: 1724.

## Supporting Information

# Grapefruit juice containing rich hydroxyl and oxygenated groups capable of transforming 1D structure of $NiCo_2O_4$ into 0D with excessive surface vacancies for promising energy conversion and storage applications

Shusheel Kumar[a], Aneela Tahira[d], Mélanie Emo[e], Brigitte Vigolo[e], Antonia Infantes-Molin[f], Amerah M. Alotaibi[b], Shoyebmohamad F Shaikh[b], and Ayman Nafady[b*], and Zafar Hussain Ibupoto[*c]

[a]Institute of Physics, University of Sindh Jamshoro, 76080, Sindh Pakistan

[b]Department of Chemistry, College of Science, King Saud University, Riyadh 11451, Saudi Arabia

[c]Institute of Chemistry, University of Sindh Jamshoro, 76080, Sindh Pakistan

[d]Institute of Chemistry, Shah Abdul Latif University Khairpur Mirs, Sindh, Pakistan

[e]Université de Lorraine, CNRS, IJL, F-54000 Nancy, France

[f]Department of Inorgnic Chemistry, Crystallography and Mineralogy. (Unidad Asociada al ICP-CSIC), Faculty of Sciences, University of Malaga, Campus de Teatinos, 29071, Malaga, Spain

*__Corresponding authors__: Zafar Hussain Ibupoto & Ayman Nafady

**Email:** zaffar.ibhupoto@usindh.edu.pk; anafady@ksu.edu.sa

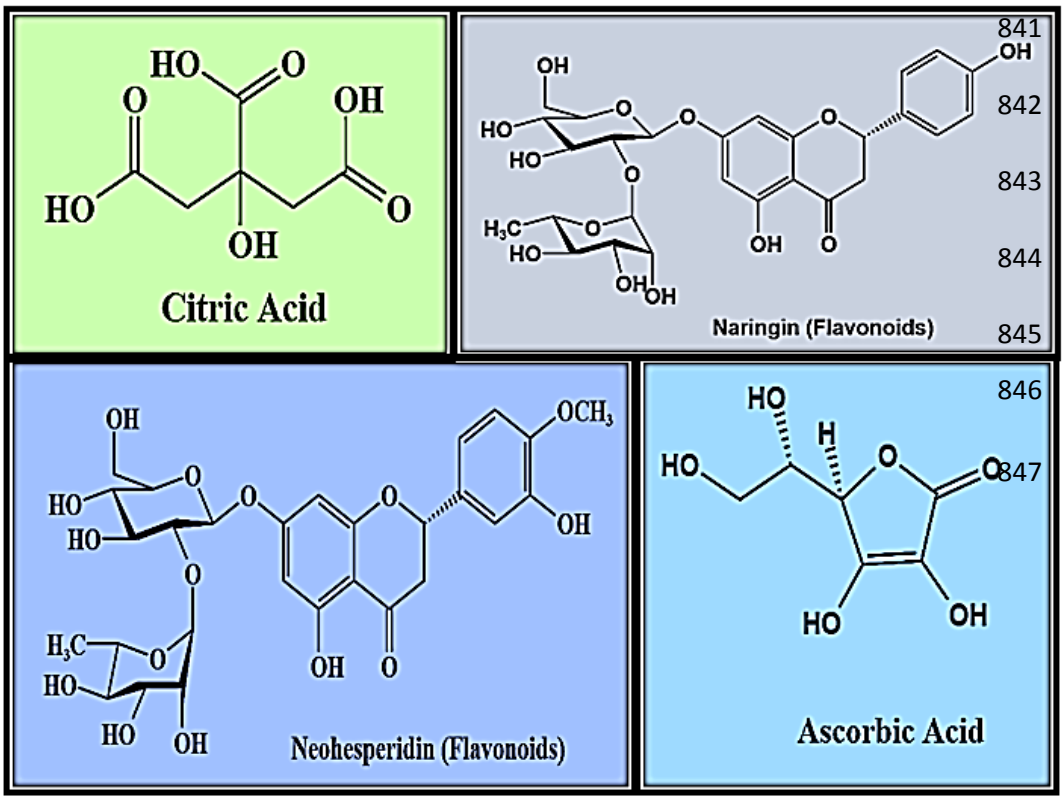

**Scheme S1:** Main chemical constituents of grapefruit juice

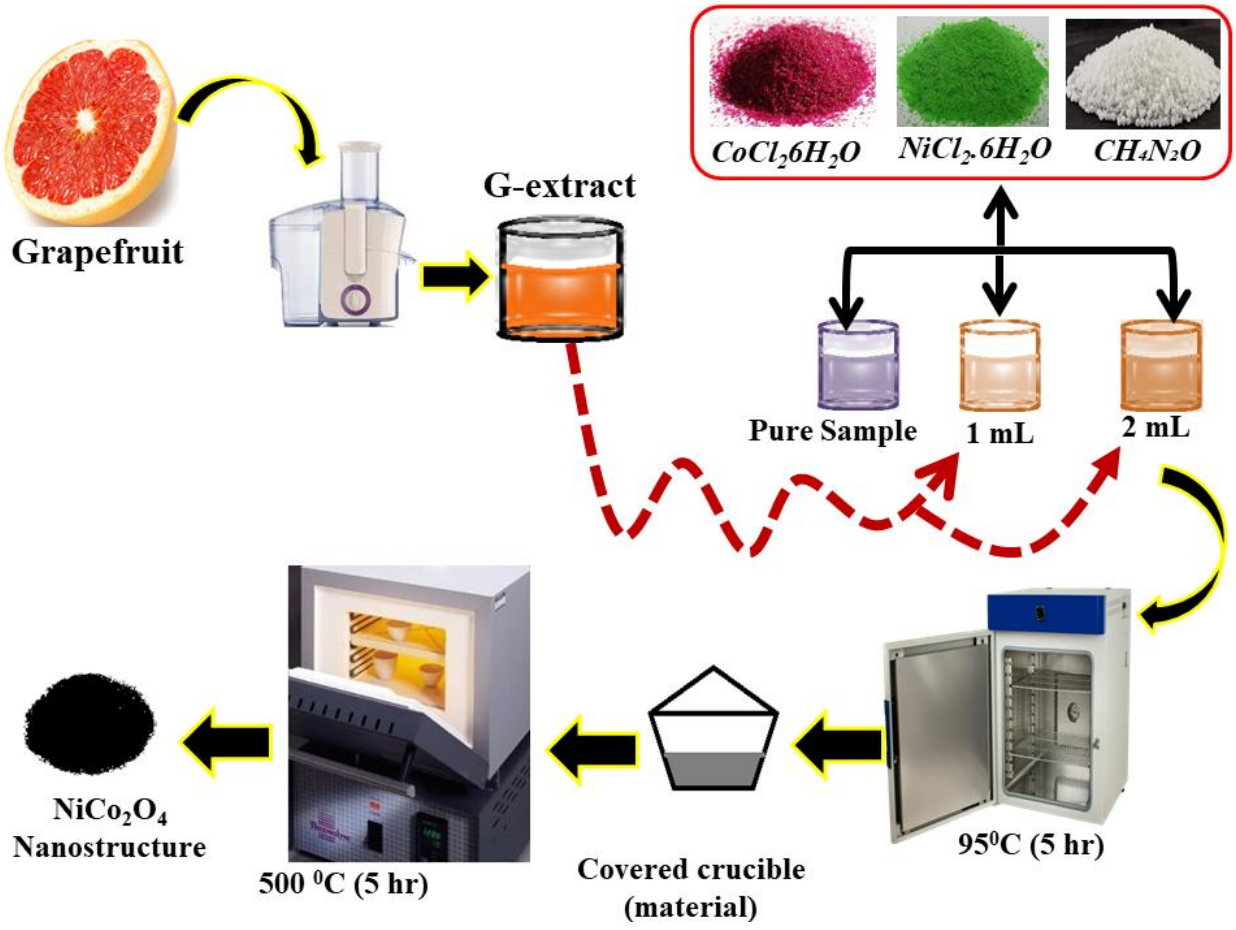


**Scheme S2:** Hydrothermal synthesis process of $NiCo_2O_4$ nanostructures using grapefruit juice.

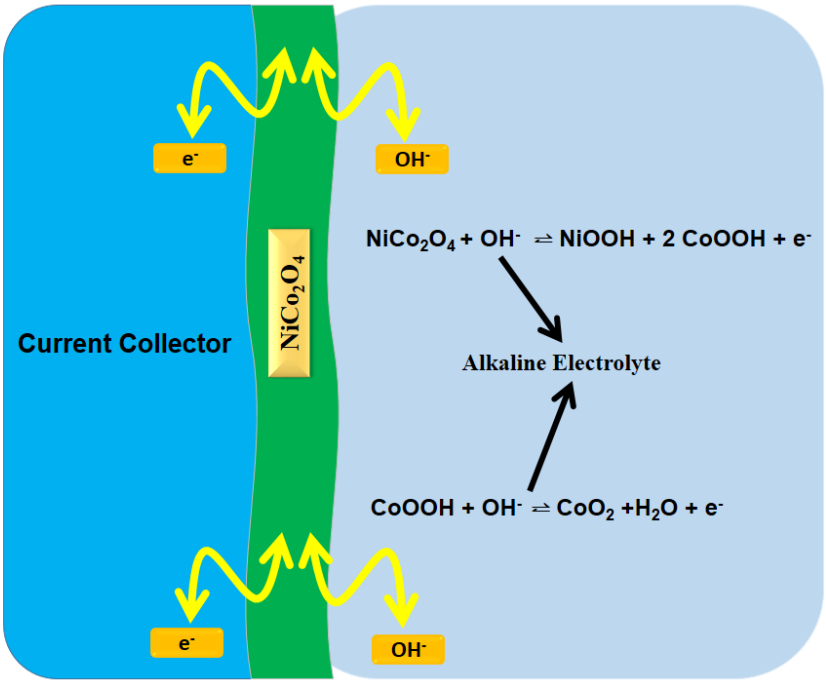


857

858 **Scheme S3:** Energy storage mechanism illustration

859

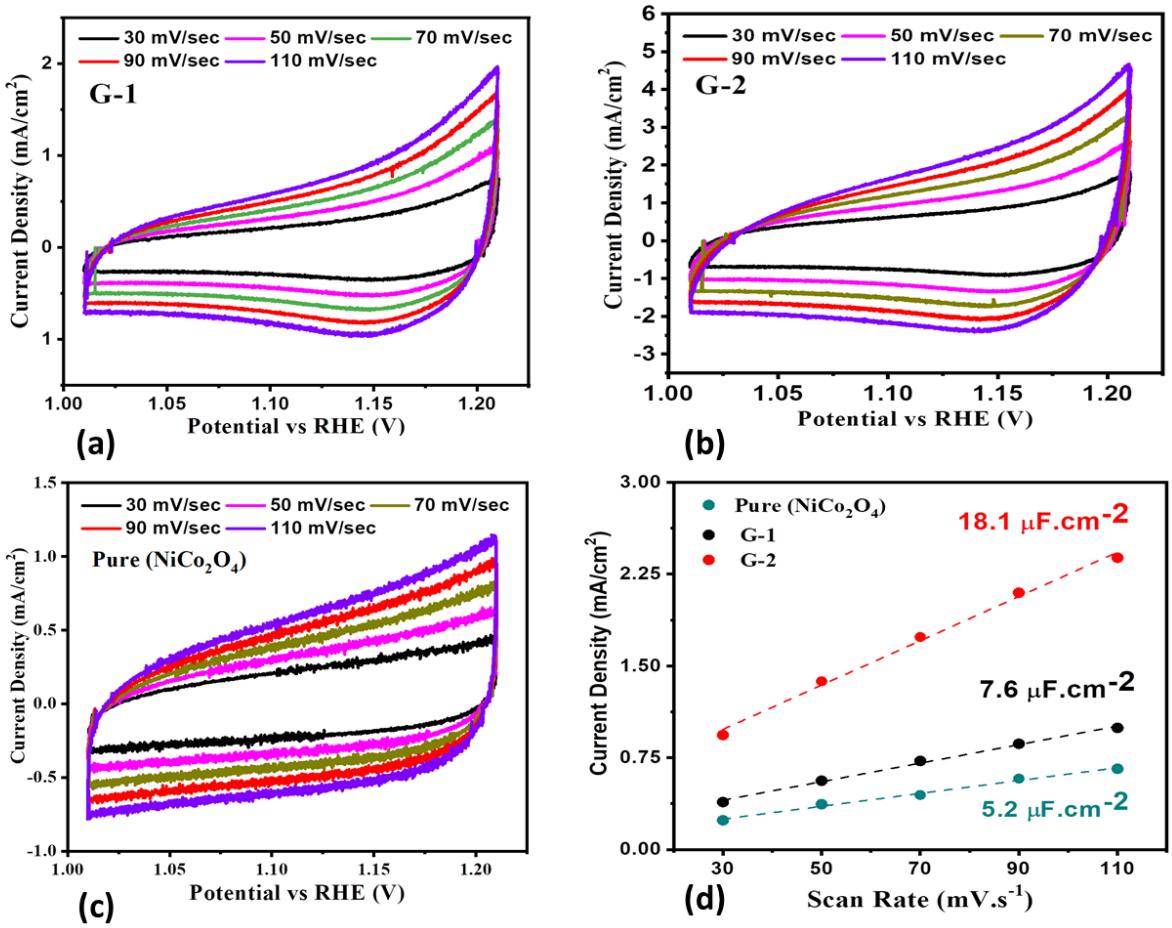


**S1:** CV curves at variosu scan rates in 1.0M KOH for (a) pristine $NiCo_2O_4$ nanostructure, (b) sample-1(G1), (c) sample-2(G2), (d) caluclated ECSA from non-Faradic region of measured CV curves for pristine $NiCo_2O_4$ nanostructure, sample-1(G1), sample-2(G2)

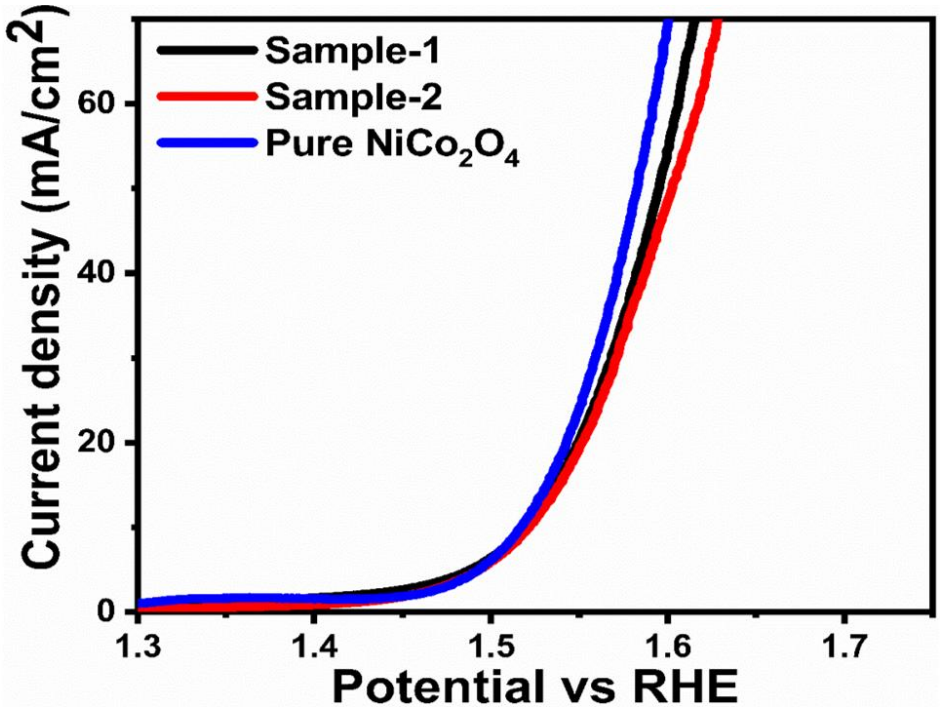


**S2:** Normalized LSV curves of of as prepared materials with their correspondign ECSA data

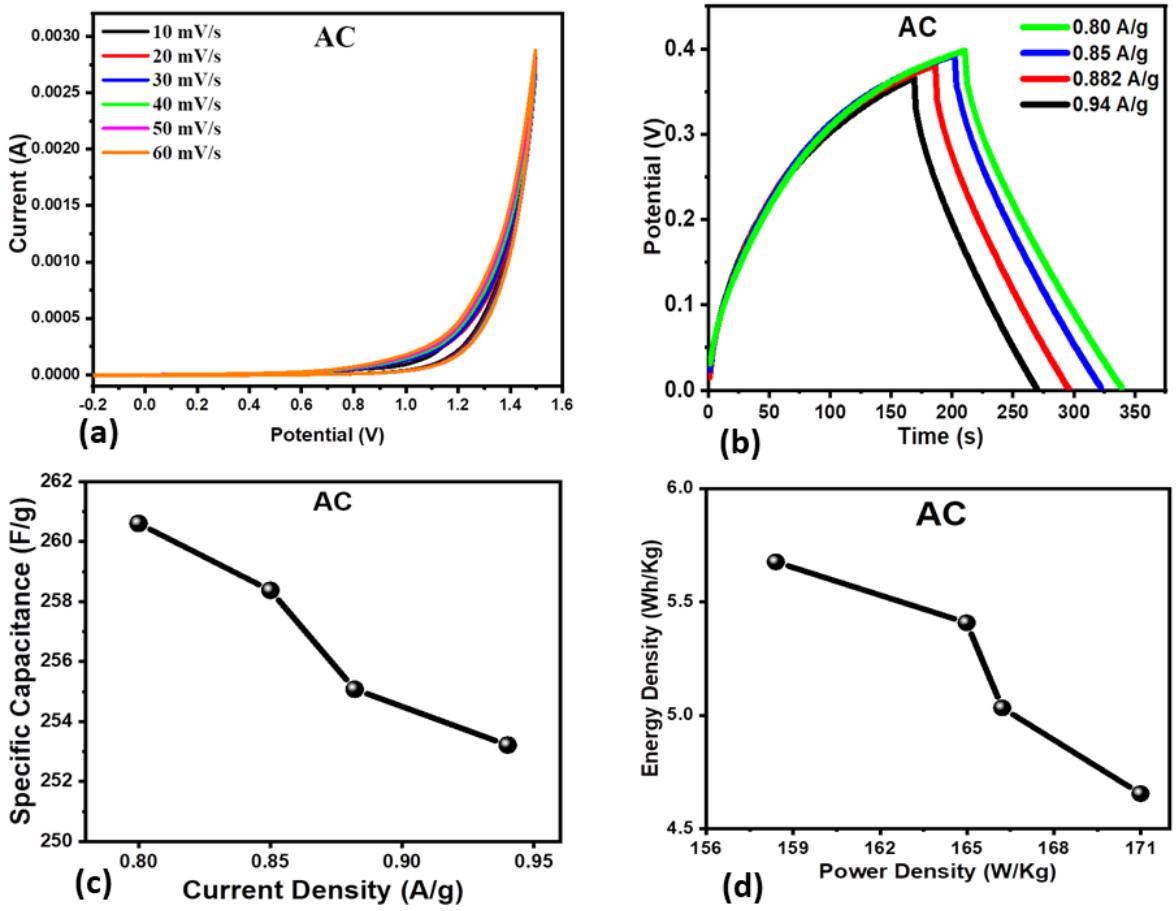

**S3:** CV curves of activated carbon (AC) at various scan rates in 3.0M KOH, (b) GCD curves of AC at different current density in 3.0M KOH, (c) specific capacitance from GCD curves of AC, (d) Energy density of AC from GCD curves in 3.0M KOH

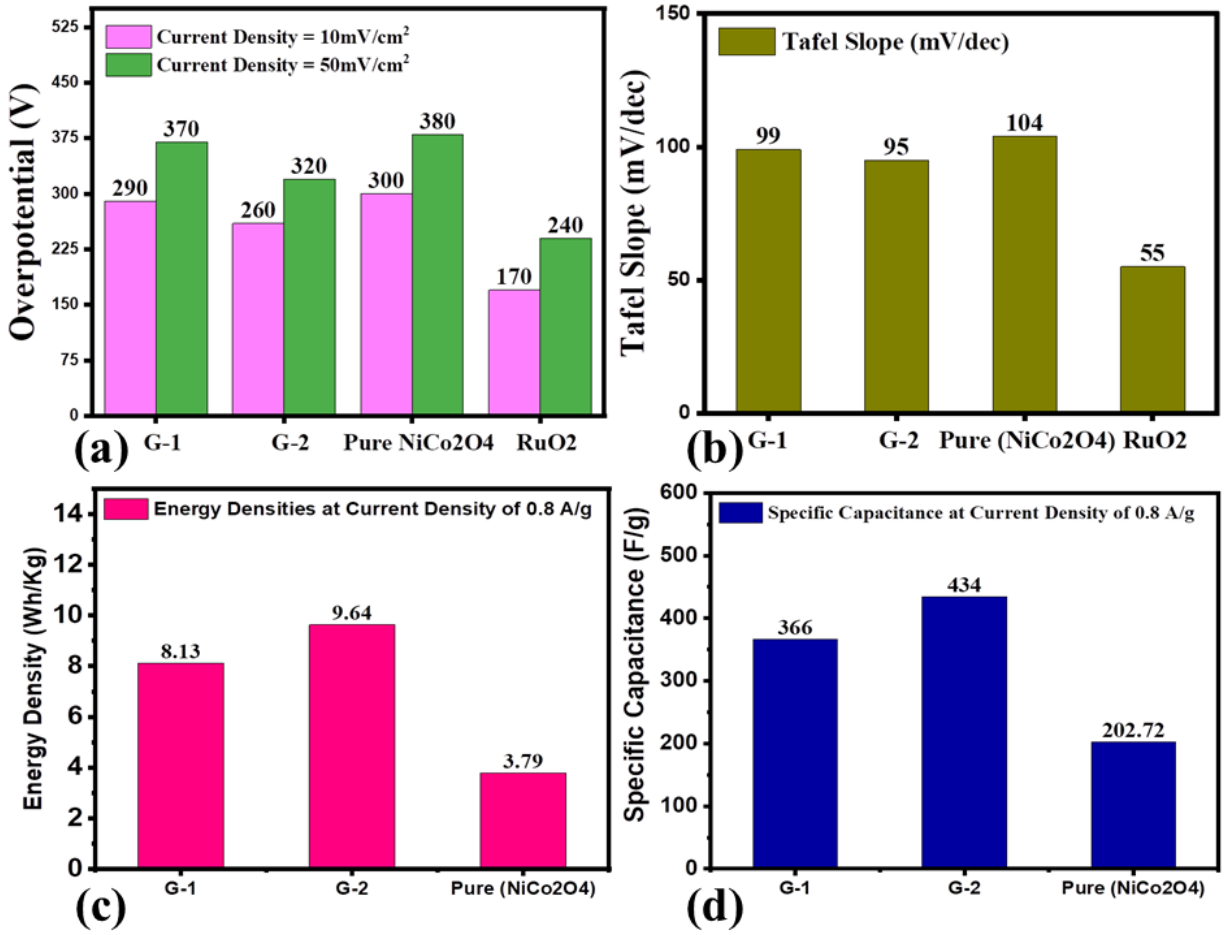


**S4:** Bar graph view (a) overpotential at 10 and 50 $mAcm^{-2}$ for $RuO_2$, pristine $NiCo_2O_4$ nanostructure, sample-1 (G1), sample-2 (G2), (b) Tafel slope for $RuO_2$, pristine $NiCo_2O_4$ nanostructure, sample-1 (G1), sample-2 (G2), (c) Energy density of supercapacitor for pristine $NiCo_2O_4$ nanostructure, sample-1 (G1), sample-2 (G2), (d) specific capacitance for pristine $NiCo_2O_4$ nanostructure, sample-1(G1), sample-2 (G2).

**Table S1:** Fitted EIS data values of charge transfer and double layer capacitance for various samples.

| | **Charge Transform Resistance (Rct in Ω)** | **Double layer Capacitor (Cdl in Farad)** |
|---|---|---|
| **Pristine** | **350** | **0.21** |
| **S-1** | **220** | **0.31** |
| **S-2** | **80** | **0.38** |

**Table S2:** Supercapacitor performance evaluation of as prepared grape fruit assisted juice $NiCo_2O_4$ nanostructure (sample-2, G2) with reported super capacitors based on $NiCo_2O_4$.

| Material | Specific Capacitance | Current Density | Potential Window | Energy Density (Wh $kg^{-1}$) | Power Density (W/kg) | Reference |
|---|---|---|---|---|---|---|
| NCO@MWCNT | 374 F/g | 2 A/g | -0.5 to 2.2V | 95 | 3964 | [1] |
| MWCNTs | 84 F/g | 0.6 A/g | -0.5 to 2.2V | 21 | 6237 | [1] |
| NCO//MWCNT | 157 F/g | 0.6 A/g | -0.5 to 2.2V | 40 | 2816 | [1] |
| NCO@MWCNT// MWCNT | 242 F/g | 0.6 A/g | -0.5 to 2.2V | 61 | 2837 | [1] |
| NiCoF | 50.0 | 1 A/g | 0 to 1 V | - | - | [2] |
| NiCuF | 44 | 1 A/g | 0 to 1 V | - | - | [2] |
| NC6 | 1294.25 | 10 A/g | 0.4 | - | - | [3] |

| | | | | | | |
|---|---|---|---|---|---|---|
| NC10 | 687.20 | 10 A/g | 0.4 | - | - | [3] |
| $NiCo_2O_4$ (Grapefruit) | 434 | 0.8 A/g | 0 to 0.4 V | 9.64 | 160 | This Work |

**Table S3:** Oxygen evolution reaction performance evaluation of as prepared grapefruit juice assisted $NiCo_2O_4$ nanostructures (sample-2, G2) with reported on $NiCo_2O_4$.

| **Catalyst** | **Overpotential @ 10 mA/cm$^2$** | **Electrolyte** | **References** |
|---|---|---|---|
| Co3O4 | 500 | 1.0 M NaOH | [4] |
| Co3O4 NPs | 363 | 1.0 M KOH | [5] |
| NiCo-LDH | 334 | 1.0 M KOH | [6] |
| Ni(Fe)OOH | 300 | 1.0 M KOH | [7] |
| Activated OM NixCoyO4 | 336 | 1.0 M KOH | [8] |
| OM NiO | 414 | 1.0 M KOH | [9] |
| $Co3O_4$ | 382 | 1.0 M KOH | [5] |
| $NiCo_2O_4$ hybrid material | 260 | 1.0 M KOH | Present Work |

# References


[1] Pathak M, Jose JR, Chakraborty B, Rout CS. High performance supercapacitor electrodes based on spinel NiCo2O4@ MWCNT composite with insights from density functional theory simulations. The Journal of Chemical Physics. 2020;152:064706.

[2] Bhujun B, Tan MT, Shanmugam AS. Study of mixed ternary transition metal ferrites as potential electrodes for supercapacitor applications. Results in Physics. 2017;7:345-53.

[3] Kaur M, Chand P, Anand H. Binder free electrodeposition fabrication of NiCo2O4 electrode with improved electrochemical behavior for supercapacitor application. Journal of Energy Storage. 2022;52:104941.

[4] Jung S, McCrory CC, Ferrer IM, Peters JC, Jaramillo TF. Benchmarking nanoparticulate metal oxide electrocatalysts for the alkaline water oxidation reaction. Journal of Materials Chemistry A. 2016;4:3068-76.

[5] Esswein AJ, McMurdo MJ, Ross PN, Bell AT, Tilley TD. Size-dependent activity of Co3O4 nanoparticle anodes for alkaline water electrolysis. The Journal of Physical Chemistry C. 2009;113:15068-72.

[6] Song F, Hu X. Exfoliation of layered double hydroxides for enhanced oxygen evolution catalysis. Nature communications. 2014;5:1-9.

[7] Yang H, Gong L, Wang H, Dong C, Wang J, Qi K, Liu H, Guo X, Xia BY. Preparation of nickel-iron hydroxides by microorganism corrosion for efficient oxygen evolution. Nature communications. 2020;11:1-9.

[8] Deng X, Öztürk S, Weidenthaler C, Tüysüz H. Iron-induced activation of ordered mesoporous nickel cobalt oxide electrocatalyst for the oxygen evolution reaction. ACS applied materials & interfaces. 2017;9:21225-33.

[9] Cheng N, Liu Q, Tian J, Sun X, He Y, Zhai S, Asiri AM. Nickel oxide nanosheets array grown on carbon cloth as a high-performance three-dimensional oxygen evolution electrode. international journal of hydrogen energy. 2015;40:9866-71.